Mathematical Models of Proprioceptors. I. Control and Transduction in the Muscle Spindle

Milana P. Mileusnic, Ian E. Brown, Ning Lan and Gerald E. Loeb

J Neurophysiol 96:1772-1788, 2006. First published May 3, 2006; doi:10.1152/jn.00868.2005

You might find this additional information useful...

This article cites 56 articles, 21 of which you can access free at:
http://jn.physiology.org/cgi/content/full/96/4/1772#BIBL

This article has been cited by 1 other HighWire hosted article:
Mathematical Models of Proprioceptors. II. Structure and Function of the Golgi Tendon Organ
M. P. Mileusnic and G. E. Loeb
J Neurophysiol, October 1, 2006; 96 (4): 1789-1802.
[Abstract] [Full Text] [PDF]

Updated information and services including high-resolution figures, can be found at:
http://jn.physiology.org/cgi/content/full/96/4/1772

Additional material and information about ***Journal of Neurophysiology*** can be found at:
http://www.the-aps.org/publications/jn

This information is current as of September 18, 2006 .

Journal of Neurophysiology publishes original articles on the function of the nervous system. It is published 12 times a year (monthly) by the American Physiological Society, 9650 Rockville Pike, Bethesda MD 20814-3991. Copyright © 2005 by the American Physiological Society. ISSN: 0022-3077, ESSN: 1522-1598. Visit our website at http://www.the-aps.org/.

Downloaded from jn.physiology.org on September 18, 2006

J Neurophysiol 96: 1772–1788, 2006.
First published May 3, 2006; doi:10.1152/jn.00868.2005.

Mathematical Models of Proprioceptors. I. Control and Transduction in the Muscle Spindle

Milana P. Mileusnic,[1] Ian E. Brown,[3] Ning Lan,[2] and Gerald E. Loeb[1]

[1]*Department of Biomedical Engineering, Alfred E. Mann Institute for Biomedical Engineering and* [2]*Department of Biokinesiology and Physical Therapy, University of Southern California, Los Angeles, California; and* [3]*Center for Neuroscience Studies, Queen's University, Kingston, Ontario, Canada*

Submitted 18 August 2005; accepted in final form 1 March 2006

Mileusnic, Milana, Ian E. Brown, Ning Lan, and Gerald E. Loeb. Mathematical models of proprioceptors. I. Control and transduction in the muscle spindle. *J Neurophysiol* 96: 1772–1788, 2006. First published May 3, 2006; doi:10.1152/jn.00868.2005. We constructed a physiologically realistic model of a lower-limb, mammalian muscle spindle composed of mathematical elements closely related to the anatomical components found in the biological spindle. The spindle model incorporates three nonlinear intrafusal fiber models (bag_1, bag_2, and chain) that contribute variously to action potential generation of primary and secondary afferents. A single set of model parameters was optimized on a number of data sets collected from feline soleus muscle, accounting accurately for afferent activity during a variety of ramp, triangular, and sinusoidal stretches. We also incorporated the different temporal properties of fusimotor activation as observed in the twitchlike chain fibers versus the toniclike bag fibers. The model captures the spindle's behavior both in the absence of fusimotor stimulation and during activation of static or dynamic fusimotor efferents. In the case of simultaneous static and dynamic fusimotor efferent stimulation, we demonstrated the importance of including the experimentally observed effect of partial occlusion. The model was validated against data that originated from the cat's medial gastrocnemius muscle and were different from the data used for the parameter determination purposes. The validation record included recently published experiments in which fusimotor efferent and spindle afferent activities were recorded simultaneously during decerebrate locomotion in the cat. This model will be useful in understanding the role of the muscle spindle and its fusimotor control during both natural and pathological motor behavior.

INTRODUCTION

The muscle spindle is a sense organ found in most vertebrate skeletal muscles. In a typical mammalian lower limb muscle, several tens (or even hundreds) of muscle spindles can be found lying in parallel with extrafusal fibers and experiencing length changes representative of muscle length changes (Barker 1962; Eldred et al. 1962). The spindle has been found to play a dominant role both in kinesthesia and in reflexive adjustments to perturbations (Hulliger 1984; Matthews 1981). Its sensory transducers (primary and secondary afferents) provide the CNS with information about the length and velocity of the muscle in which the spindle is embedded. The spindle provides the main source of proprioceptive feedback for spinal sensorimotor regulation and servocontrol. At the same time that the spindle supplies the CNS with afferent information, it also receives continuous control through specialized fusimotor efferents (static and dynamic fusimotor efferents) whose task is to shift the spindle's relative sensitivities over the wide range of lengths and velocities that occur in various natural tasks (Banks 1994; Matthews 1962).

The spindle consists of three types of intrafusal muscle fibers: long nuclear bag_1 and bag_2 fibers and shorter chain fibers (Fig. 1*A*) (Boyd et al. 1977). Typically, one bag_1, one bag_2, and about four to 11 chain fibers lie in parallel within a spindle (Boyd and Smith 1984). The bag_1 fiber is the only fiber that has dynamic fusimotor efferent endings located on it and is primarily responsible for the velocity sensitivity of the spindle. The bag_2 and chain fibers receive static fusimotor control and contribute mainly to length sensitivity. Located in the equatorial region of all three types of intrafusal fibers are primary afferent endings responsible for supplying the CNS with the length and velocity information from the muscle. The more slowly conducting secondary afferent has its endings located more eccentrically, on only the bag_2 and chain fibers, and is responsible for supplying CNS with primarily length information.

Because of the difficulty of accurately recording afferent and especially fusimotor activity during motor behavior, theories of motor control usually rely on assumptions about spindle activity. Throughout the years, several attempts have been made to formalize these assumptions in mathematical models capable of accurately capturing spindle activity over the wide range of kinematic and fusimotor conditions in which spindles naturally operate. These modeling approaches involved either transfer functions (Chen and Poppele 1978; Matthews and Stein 1969), nonlinear functions based on curve-fitting (Houk et al. 1981; Maltenfort and Burke 2003), or reduction to constituent anatomical components (Hasan 1983; Lin and Crago 2002; Rudjord 1970; Schaafsma et al. 1991). As a consequence of the complex nature of spindle responses, the earliest models attempted to model primarily afferent activity in the absence of fusimotor activation, with the exception of Hasan (1983). Only recently have several more complex spindle models, incorporating the fusimotor effects on afferent activity, been developed (Lin and Crago 2002; Maltenfort and Burke 2001; Schaafsma et al. 1991). Although each new model has enhanced our understanding of how the spindle operates, there are still certain aspects of spindle behavior that these models fail to capture (such as occlusion between transduction regions

Address for reprint requests and other correspondence: M. P. Mileusnic, Alfred E. Mann Institute for Biomedical Engineering, Department of Biomedical Engineering, University of Southern California, 1042 West 36th Place, Room B11, Los Angeles, CA 90089-1112 (E-mail: mileusni@usc.edu).

The costs of publication of this article were defrayed in part by the payment of page charges. The article must therefore be hereby marked "*advertisement*" in accordance with 18 U.S.C. Section 1734 solely to indicate this fact.

0022-3077/06 $8.00 Copyright © 2006 The American Physiological Society

Downloaded from jn.physiology.org on September 18, 2006

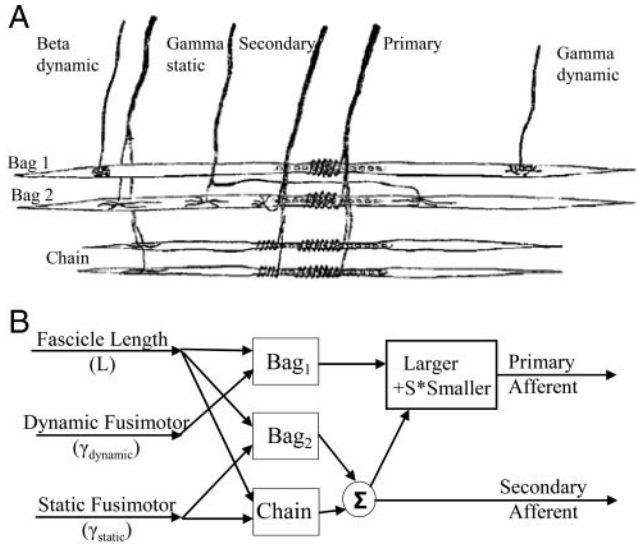

FIG. 1. A biological muscle spindle and the structure of the spindle model. *A*: a biological muscle spindle consists of 3 types of intrafusal fibers that receive several fusimotor inputs (gamma static and dynamic) while giving rise to primary (Ia) and secondary (II) afferent (modified from Bakker 1980). *B*: spindle model consists of 3 intrafusal fiber models; it receives 3 inputs (fascicle length, in terms of optimal length L_0, and static and dynamic fusimotor drives) to produce primary and secondary afferent firing.

and temporal dynamics of changing fusimotor input; see DISCUSSION).

We constructed a physiologically realistic model of the spindle that is composed of mathematical elements closely related to the anatomical components found in the biological spindle and their physiological properties. Its parameters were optimized using cat soleus muscle afferent data recorded during a variety of kinematic and fusimotor conditions. The emergent behavior of the model is shown to account well for the complete range of complex phenomena described in various experiments. The model was validated against recently reported data on medial gastrocnemius afferent activity during decerebrate locomotion of the cat that include direct recordings of related fusimotor efferent activity. Preliminary reports of this study were previously published (Mileusnic et al. 2001, 2002).

METHODS

In this section we will initially concentrate on the equations and individual terms that describe the spindle model and how they are related to the current understanding of the biological system. Afterward, the implementation of the model will be discussed and will include the criteria for selecting the afferent records and techniques used to perform the parameter optimization.

The spindle model

The spindle model is composed of three intrafusal fiber models (nuclear bag_1 and bag_2 fibers and chain fiber) and two afferent firing summation models (primary and secondary afferent firing models) (see Fig. 1). The same basic function was used to model all three intrafusal fiber types, with different coefficient values to account for their different physiology and effects. Each intrafusal fiber model responds to two inputs: fascicle length (L; in units of L_0, which represents the optimal muscle fascicle length) and the relevant fusimotor drive [in the case of bag_1 fiber it is dynamic fusimotor drive ($\gamma_{dynamic}$), whereas in the case of bag_2 it is chain static fusimotor drive (γ_{static}) (Fig. 1*B*)]. The spindle model generates two outputs: primary (Ia) and secondary (II) afferent activity. The primary afferent response results from the contributions of all three intrafusal fiber models on which the primary afferent receptor has transduction endings. The secondary afferent receives inputs from only the bag_2 and chain intrafusal fiber models.

In the next two major sections we will develop the spindle model in stages. First we will describe the general intrafusal fiber model. This section of model development is further subdivided into the three components that deal with fusimotor activation, the mechanics of stretch within the intrafusal fiber, and finally sensory transduction from stretch to afferent endings. Second, we describe the afferent firing model that deals with nonlinear summation between the intrafusal fibers' transduction regions.

The intrafusal fiber model

All the intrafusal fiber models share the same general structure, a modified version of McMahon's spindle model (McMahon 1984), which has its origins in the earlier work by Crowe (1968, 1970). The relative importance of model parameters differs for three intrafusal fiber models to account for the different properties of three fiber types (see Table 1 and Fig. 2). The form of the intrafusal fiber model was also influenced by recent improvements in the modeling of extrafusal mechanics (Brown and Loeb 2000; Brown et al. 1996b, 1999).

BACKGROUND. The linear spindle model suggested by McMahon (1984) makes no distinction between different intrafusal fibers, but rather the fibers are lumped together into one spindle model. Similar to the structure of intrafusal fibers found in the biological spindle, McMahon's spindle model consists of two regions, sensory and polar (a modified version is shown in Fig. 2). The sensory (transduction) region contains afferent endings wrapped around it. Stretch of this region results in distortion of afferent endings, depolarization of their membranes, and increase in the rate of action potential firing (Boyd and Smith 1984). McMahon modeled transduction as a spring whose stretch is proportional to afferent firing. The rest of the intrafusal fiber on either side of the sensory region is called the polar region, constituting essentially a striated muscle fiber innervated by fusimotor endings; for simplicity, the two polar regions of the biological spindle are combined into one polar region for the model. McMahon used a typical Hill model for the polar region, including a passive spring in parallel with a contractile element, which further consists of an active force generator and a damping element. The contractile element was designed to represent the properties of the spindle that change in response to fusimotor activation, although these coefficients were never explicitly modeled by McMahon.

FUSIMOTOR ACTIVATION. A biochemical Hill-type equation was used to convert the actual fusimotor frequency [$\gamma_{dynamic}$ or γ_{static} in pulses per second (pps)] to an equivalent activation level ($f_{dynamic}$ or f_{static}, defined within range 0 to 1). This allows each intrafusal fiber model to capture the saturation effects that take place at high fusimotor stimulation frequencies as observed in isolated, identified fibers (bag_1: $freq_{bag_1}$ = 100 pps; bag_2: $freq_{bag_2}$ = 100 pps; chain: $freq_{chain}$ = 150 pps; Boyd 1976). In addition, the model incorporates the different temporal properties of intrafusal fiber responses that were measured previously for individual intrafusal fibers in response to step changes in fusimotor activation (Boyd et al. 1977). These different temporal properties are thought to arise from differences in the spread of activation in twitch muscle fibers that propagate action potentials (including chain fibers) versus tonic muscle fibers where synaptic depolarization spreads electrotonically (including bag fibers; Boyd 1976), as well as being related to differences in calcium kinematics. To model these differences, low-pass filters between the fusimotor inputs and the equivalent activation levels were introduced for the two relatively slow bag intrafusal fibers (see APPENDIX 1, *A*). The following

Downloaded from jn.physiology.org on September 18, 2006

TABLE 1. *Spindle model parameters*

Parameter	Parameter Definition	Bag_1	Bag_2	Chain
K^{SR}	Sensory region spring constant [FU/L_0]	10.4649	10.4649	10.4649
K^{PR}	Polar region spring constant [FU/L_0]	0.1500	0.1500	0.1500
M	Intrafusal fiber mass [FU/(L_0/s^2)]	0.0002	0.0002	0.0002
B_0	Passive damping coefficient [FU/(L_0/s)]	0.0605	0.0822	0.0822
β_1	Coef. of damping due to dyn. fusimotor input [FU/(L_0/s)]	0.2592		
β_2	Coef. of damping due to stat. fusimotor input [FU/(L_0/s)]		−0.0460	−0.0690*
Γ_1	Coef. of force generation due to dyn. fusimotor input [FU]	0.0289		
Γ_2	Coef. of force generation due to stat. fusimotor input [FU]		0.0636	0.0954*
C_L	Coef. of asymmetry in F–V curve during lengthening	1	1	1
C_S	Coef. of asymmetry in F–V curve during shortening	0.4200	0.4200	0.4200
X	Percentage of the secondary afferent on sensory region		0.7**	0.7**
L_N^{SR}	Sensory region threshold length (L_0)	0.0423	0.0423	0.0423
L_N^{PR}	Polar region threshold length (L_0)		0.89**	0.89**
G	Term relating the sensory region's stretch to afferent firing	20,000	10,000 (7,250)	10,000 (7,250)
a	Nonlinear velocity dependence power constant	0.3	0.3	0.3
R	Fascicle length below which force production is zero (L_0)	0.46	0.46	0.46
L_0^{SR}	Sensory region rest length (L_0)	0.04	0.04	0.04
L_0^{PR}	Polar region rest length (L_0)	0.76	0.76	0.76
$L_{secondary}$	Secondary afferent rest length (L_0)		0.04	0.04
τ	Low-pass filter time constant (see APPENDIX 1) (s)	0.149	0.205	
freq	Constant relating the fusimotor frequency to activation	60	60	90
p	Power constant relating the fusimotor frequency to activation	2	2	2

FU is force unit. Values in FUs are arbitrary because they can be scaled by a constant without a change in the model's behavior. *Chain fiber values that needed to be scaled from bag_2 values because of different fusimotor saturation frequencies for two fibers (bag_2 values × 1.5). Values in parentheses are values used to model the secondary afferent. ** Parameters that need to be adjusted to capture the variability in secondary afferent response across different spindles. Note that the parameter values below the L_N^{PR} parameter were extracted directly from the experimental literature (see text).

equations were used to convert the actual fusimotor frequency ($\gamma_{dynamic}$ or γ_{static}) to an equivalent activation level ($f_{dynamic}$ or f_{static}) for three types of intrafusal fibers

$$\begin{cases} \dfrac{df_{dynamic}}{dt} = \dfrac{\dfrac{\gamma^P_{dynamic}}{\gamma^P_{dynamic} + freq^P_{bag_1}} - f_{dynamic}}{\tau} & \text{for } bag_1 \text{ fiber, which saturates at about 100 pps} \\ \dfrac{df_{static}}{dt} = \dfrac{\dfrac{\gamma^P_{static}}{\gamma^P_{static} + freq^P_{bag_2}} - f_{static}}{\tau} & \text{for } bag_2 \text{ fiber, which saturates at about 100 pps} \\ f_{static} = \dfrac{\gamma^P_{static}}{\gamma^P_{static} + freq^P_{chain}} & \text{for chain fiber, which saturates at about 150 pps} \end{cases} \quad (1)$$

MECHANICS OF SENSORY AND POLAR REGIONS. With the intention of keeping our model as simple as possible, we initially assumed our intrafusal fiber model to have McMahon's intrafusal fiber model structure. By manually tuning all the parameters in the model, the model's ability to accurately account for experimentally observed spindle afferent activity during a variety of kinematic conditions and fusimotor activations was assessed and the potential need for additional terms was identified. Addition of every further term involved extensive testing of the model's performance to reduce the danger of overcomplicating the model with terms whose functions were unknown.

Similar to McMahon's spindle model, our final model incorporates a sensory region of each intrafusal fiber model as a pure elastic element with a spring constant K^{SR}. The tension within this region is equal to

$$T = K^{SR} \times [(L - L^{PR}) - L_0^{SR}] \quad (2)$$

where L is fascicle length, L^{PR} is polar region length, and L_0^{SR} is the unloaded sensory region length, all in units of L_0.

The polar region is modeled as a spring with a spring constant K^{PR} and a parallel contractile element that consists of an active force generator and a damping element, both of whose properties are modulated by fusimotor input. The tension within this region is equal to

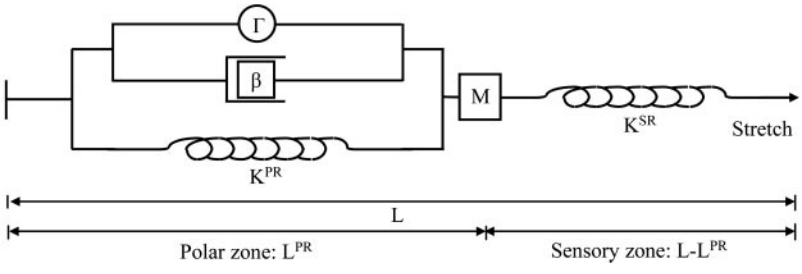

FIG. 2. Intrafusal fiber model. All intrafusal fibers consist of polar and sensory zones with qualitatively identical mechanical components. For each fiber model the stretch in the sensory and polar regions is calculated to determine its contribution to the firing of each afferent. Model parameters for each intrafusal fiber type are provided in Table 1.

Downloaded from jn.physiology.org on September 18, 2006

$$T = M \times \ddot{L}^{PR} + \beta \times C \times (L^{PR} - R) \times \text{sign}(\dot{L}^{PR}) \times \text{abs}\,(\dot{L}^{PR})^{a} + K^{PR} \times (L^{PR} - L_0^{PR}) + \Gamma \quad (3)$$

where

$$\beta = \beta_0 + \beta_1 \times f_{dynamic} + \beta_2 \times f_{static} \quad (4)$$

and

$$\Gamma = \Gamma_1 \times f_{dynamic} + \Gamma_2 \times f_{static} \quad (5)$$

M refers to the intrafusal fiber mass required for computational stability in a series-elastic system with velocity-dependent contractility (Brown et al. 1996b). L_0^{PR} is a polar region's rest length. β represents the polar region's damping term; increases in β result in increases in the velocity sensitivity of the primary afferent, which plays an important role in modulating the spindle's behavior during dynamic fusimotor stimulation of bag_1 fiber (β_1) (the only intrafusal fiber receiving dynamic fusimotor drive) (Crowe and Matthews 1964). By contrast, static fusimotor activation produces a small decrease in β (note that β_2 is negative) (Crowe and Matthews 1964). Γ is defined as the active-state force generator term; increases in Γ result in an increase in the bias activity of the dependent afferent. Static fusimotor input causes a sustained, strong contraction within the bag_2 and chain polar regions ($\Gamma_2 \times f_{static}$), producing a stretch in the sensory region and a bias in the afferent activity. Dynamic fusimotor input produces a similar but much weaker effect ($\Gamma_2 \times f_{dynamic}$). The model incorporates the experimentally observed nonlinear velocity dependency of the spindle's afferent response and was modeled with the velocity power term $(\dot{L}^{PR})^{a}$ (Houk et al. 1981; Prochazka and Gorassini 1998). C is a constant describing the experimentally observed asymmetric effect of velocity on force production during lengthening and shortening. Although this asymmetry has been observed directly only in extrafusal striated muscle (Scott et al. 1996), we have assumed its existence also in the case of the intrafusal fiber's contractile polar region. C was set to unity during polar region lengthening ($C = C_L = 1$) and to C_S during shortening ($C = C_S$). Finally, the model incorporates the length dependency of the force–velocity relationship (term $L^{PR} - R$), where an increase in fascicle length results in increased slope of the force–velocity relationship for slow to moderate velocities. This effect, observed in extrafusal fibers, is believed to result from the influence of myofilament lattice spacing on cross-bridge kinetics (Brown et al. 1999). Under most physiological conditions the sarcomere length of the intrafusal fiber's polar region tends to follow that of extrafusal fibers (extrafusal sarcomere: Scott et al. 1996; intrafusal sarcomere: Barker 1974; Bessou et al. 1975; Boyd 1976; Poppele and Quick 1981), so the extrafusal fiber measurements were used to estimate the length (R) of the polar region of intrafusal fibers for this effect (assuming that length changes in sensory region are minor comparing to those in the polar region; see *Implementation of the spindle model and parameter determination*).

INTRAFUSAL FIBER CONTRIBUTIONS TO AFFERENT FIRING. In our spindle model, the stretches in the sensory and polar regions are independently calculated for each intrafusal fiber to determine their potential contributions to afferent firing. Because tensions in *Eqs. 2* and *3* are the same, the sensory region's equation for tension (*Eq. 2*) was rearranged to express polar region length (L^{PR}) in terms of tension (T) and fascicle length (L). This polar region length was then substituted into *Eq. 3* to obtain a second-order differential equation of tension in terms of fascicle length

$$\ddot{T} = \frac{K^{SR}}{M} \times \left[\begin{array}{c} C \times \beta \times \text{sign}\left(\dot{L} - \frac{\dot{T}}{K^{SR}}\right) \times \text{abs}\left(\dot{L} - \frac{\dot{T}}{K^{SR}}\right)^{a} \times \left(L - L_0^{SR} - \frac{T}{K^{SR}} - R\right) \\ + K^{PR} \times \left(L - L_0^{SR} - \frac{T}{K^{SR}} - L_0^{PR}\right) + M \times \ddot{L} + \Gamma - T \end{array} \right] \quad (6)$$

Because the primary afferent endings are located on the sensory regions of all three intrafusal fibers, the stretch in the sensory region of each intrafusal fiber is calculated (T/K^{SR}). Once the afferent endings are stretched passed a certain sensory region length (sensory region threshold length: L_N^{SR}) the ion channels open and depolarization/impulse generation takes place. The stretch above the threshold length is scaled by a constant G (the term that relates the stretch of the intrafusal fiber's sensory region to primary afferent firing; see *Implementation of the model and parameter determination*) to obtain the intrafusal fiber's contribution to the activity of the primary afferent (before nonlinear intrafusal fiber firing summation between bag_1 and combined bag_2 and chain fiber models; for more details see next section)

$$\text{Afferent\_potential}_{primary} = G \times \left[\frac{T}{K^{SR}} - (L_N^{SR} - L_0^{SR}) \right] \quad (7)$$

Contrary to the primary afferent endings, the secondary afferent transduction zones are located more eccentrically, straddling both sensory and polar regions of bag_2 and chain intrafusal fibers. Therefore action potential generation reflects the stretch in both sensory and polar regions

$$\text{Afferent\_potential}_{secondary} = G \times \left\{ \begin{array}{l} X \times \frac{L_{secondary}}{L_0^{SR}} \times \left[\frac{T}{K^{SR}} - (L_N^{SR} - L_0^{SR}) \right] \\ + (1 - X) \times \frac{L_{secondary}}{L_0^{PR}} \times \left(L - \frac{T}{K^{SR}} - L_0^{SR} - L_N^{PR} \right) \end{array} \right\} \quad (8)$$

X represents the percentage of the secondary afferent located on the sensory region, which can vary among spindles. The stretch within the part of the secondary afferent that is located on the sensory region is obtained by multiplying X by sensory region stretch above the sensory region threshold length (L_N^{SR}) and normalizing it by the ratio of the secondary afferent rest length ($L_{secondary}$) and sensory region rest length (L_0^{SR}). The stretch within the part of the secondary afferent located on the polar region is similarly obtained. The polar region length at and above which secondary afferent sensory endings are stretched is defined as the polar region threshold length (L_N^{PR}). Once the stretches of the secondary afferent portions that are located on both sensory and polar regions are obtained, they are summed together and multiplied by G to obtain the intrafusal fiber contribution to secondary afferent firing.

Afferent firing model

The output of the primary afferent is captured by nonlinear summation between the bag_1 and combined bag_2 plus chain intrafusal fiber outputs, to account for the effect of partial occlusion that has been observed in primary afferents during simultaneous static and dynamic fusimotor stimulation (Banks et al. 1997; Carr et al. 1998; Fallon et al. 2001). Such combined fusimotor stimulation produces an afferent response that is greater than the larger of the individual responses (during either static or dynamic fusimotor stimulation) but smaller than their sum. Although the mechanism responsible for the occlusion is still debated (Banks et al. 1997; Carr et al. 1998; Fallon et al. 2001; Proske and Gregory 2002), one likely explanation assumes

Downloaded from jn.physiology.org on September 18, 2006

the existence of two impulse generators in the spindle afferent. One impulse generator is believed to be located on the bag_1 fiber, whereas the second combines generator potentials from receptors on both the bag_2 and chain fibers (Banks et al. 1997; Carr et al. 1998; Celichowski et al. 1994; Fallon et al. 2001). The primary afferent firing results from competition between these two impulse generators in which the dominant generator wins and suppresses all activity in the weaker generator by resetting. Although that would produce total occlusion, the mechanism responsible for partial occlusion is believed to involve spread of transduction current between the suppressed and dominant generator, resulting in increased impulse generation at the dominant site. Regardless of the exact mechanism, the effect has been well described experimentally and was incorporated into the model. The driving potentials produced by bag_1 and combined bag_2 and chain intrafusal fibers are compared and the larger of the two plus a fraction (S) of the smaller are summed to obtain the primary afferent firing. The secondary afferent output (which is not influenced by bag_1 receptors) is obtained from the simple summation of the outputs of bag_2 and chain intrafusal fiber models.

Implementation of the spindle model and parameter determination

The anatomical and mathematical structure of the spindle model was embodied as a set of nested blocks in the MATLAB Simulink modeling environment. First, a number of the model parameters were estimated and set directly from experimental measurements. The remainder of the parameters were then fit using standard least-squares fitting algorithms.

DIRECT PARAMETER ESTIMATION. The values of a number of model parameters, described below, were estimated directly based on a variety of previously published data. These parameters were estimated directly rather than leaving them as free parameters because in each case there was enough experimental evidence to justify such a direct approach.

The term "a," representing the nonlinear velocity dependency of afferent firing, was set to value 0.3 (Houk et al. 1981). We found a velocity power term of 0.3 (Houk et al. 1981) to produce a better fit when capturing the increase in the spindle primary's dynamic response during three velocities of ramp stretch than 0.5–0.6 as suggested by Prochazka and Gorassini (1998).

Based on Boyd's figures, we estimated "L_0^{SR}," "L_0^{PR}," and "$L_{secondary}$," which represent the sensory and polar regions' spring rest lengths and secondary afferent rest length (Boyd 1976). By dissecting the individual cat's spindle and examining it under the microscope, Boyd found that at the spindle's rest length, some 5% of its length belongs to the sensory region (where primary endings are located) and 95% to the polar region. The length of the secondary afferent ending that spans both the sensory and polar regions is roughly 5% of the total spindle's rest length. To obtain these percentages in terms of optimal fascicle length we estimated the spindle's rest length from the soleus fascicle slack length ($0.8L_0$) (Scott et al. 1996). Therefore "L_0^{SR}," "L_0^{PR}," and "$L_{secondary}$" were estimated to be $0.04L_0$, $0.76L_0$, and $0.04L_0$, respectively.

"R" represents the polar region length above which the lattice spacing of the myofilaments has effects on the cross-bridge kinetics that drive the force–velocity relationship. We assumed that this basis length would be similar for intrafusal and extrafusal fibers. In the case of extrafusal fibers, the effect of myofilament lattice spacing on cross-bridge kinetics was observed for fascicle lengths between $0.8L_0$ and $1.2L_0$, although the data suggest that the effect exists for the shorter fascicle lengths as well (see Fig. 3*C* in Brown et al. 1999). By extracting the suggested force–fascicle length curve, we estimated that this effect exists for fascicle lengths $\gtrsim 0.5L_0$. To determine the polar region length at $0.5L_0$ fascicle length, we first needed to estimate the sensory region length. Because the evidence suggests that length changes in the sensory region are almost negligible compared with the length changes of the polar region (Boyd 1976), we assumed that at $0.5L_0$ fascicle length, the sensory region is approximately equal to its rest length ($0.04L_0$). Therefore the polar region length at $0.5L_0$ fascicle length was estimated to be $0.46L_0$ ("R").

"G," the term that relates the stretch of the intrafusal fiber's sensory endings to primary afferent firing, was estimated based on experimental data on cat tenuissimus muscle (Boyd 1976; Boyd et al. 1977) in the presence of maximal dynamic fusimotor stimulation; the bag_1 sensory endings stretch by some 2–8% (scaling it to units of L_0: 5% of primary sensory ending rest length $= 0.05 \times 0.04L_0 = 0.002L_0$) while generating about 40 pps of the primary afferent firing. By combining these two values, the "G" term for bag_1 fiber was estimated [G(for bag_1) $= 40$ pps/$0.002L_0 \approx 20{,}000$ pps/L_0]. Similarly, we obtained the "G" value for the combined bag_2 and chain intrafusal fiber model, where maximal observed stretch during maximal static fusimotor stimulation of bag_2 and chain was 12–30 and 15–20%, respectively (average 19% of sensory region rest length $= 0.19 \times 0.04L_0 = 0.0076L_0$) (Boyd 1976; Boyd et al. 1977), and primary afferent firing about 150 pps (Boyd 1986) [G(for bag_2&chain, primary) $= 150$ pps/$0.0076L_0 \approx 20{,}000$ pps/L_0]. In the case of the secondary afferent endings, the maximal observed stretch during maximal static fusimotor stimulation of bag_2 and chain fibers was comparable to the primary afferent case (Boyd 1976; Boyd et al. 1977), whereas the secondary firing observed at this stretch was about 110–115 pps (Boyd 1986) [G(for bag_2&chain, secondary) $= 110$ pps/$0.0076L_0 \approx 14{,}500$ pps/L_0].

The term "S" that represents the amount of partial occlusion that occurs in primary afferent firing also originated from direct experimental measurements (Fallon et al. 2001). Although there is some experimental evidence suggesting a length dependency to S, at this point, the data are very limited and noisy. As such, we have assumed that S is constant ($S = 0.156$), with the acknowledgment that if further data support an actual length dependency to S, then the model will need to be so modified.

The parameters that are used in mapping the fusimotor stimulation frequency to the model's fusimotor activation ("p," "$freq_{bag_1}$," "$freq_{bag_2}$," and "$freq_{chain}$") were estimated based on Boyd's measurements of the intrafusal fiber's polar region contraction in response to different fusimotor stimulation frequencies (Boyd 1976). Because the chain fiber's measurements were obtained at relatively high frequencies, we used these data to estimate the Hill-equation parameters for chain fiber and then modified them for other two fibers to account for their different saturation frequencies. We should mention that, although limited experimental data suggest that fusimotor stimulation above the saturation frequencies [100 Hz for bag_1 ($f_{dynamic} = 0.735$) and bag_2 ($f_{static} = 0.735$); 150 Hz for chain ($f_{static} = 0.735$)] will have little or no additional effect beyond that observed at the saturation frequency, our model actually has a slowly increasing effect because of the nature of the Hill equation. Although it was possible to correct this by introducing some nonlinearity in the model we chose not to do so to avoid complications during the model inversion (see DISCUSSION). We believe that this does not represent a limitation of our model because fusimotor neurons usually fire at frequencies below the saturation level (see DISCUSSION).

DATA SELECTION FOR FREE PARAMETER OPTIMIZATION. In a series of experiments during the 1960s and 1970s, the activities of identified primary and secondary afferents were recorded from isolated or partly isolated spindles from soleus muscle of the cat. We used essentially the same published records that were used in previous spindle modeling studies (i.e., Lin and Crago 2002; Maltenfort and Burke 2003; Schaafsma et al. 1991) to represent afferent activity during a broad range of experimentally controlled kinematic and fusimotor conditions. Afferent activity records during different velocities of ramp, triangular, and sinusoidal stretches under various constant fusimotor drives were used to develop and tune the model (Crowe and Matthews

Downloaded from jn.physiology.org on September 18, 2006

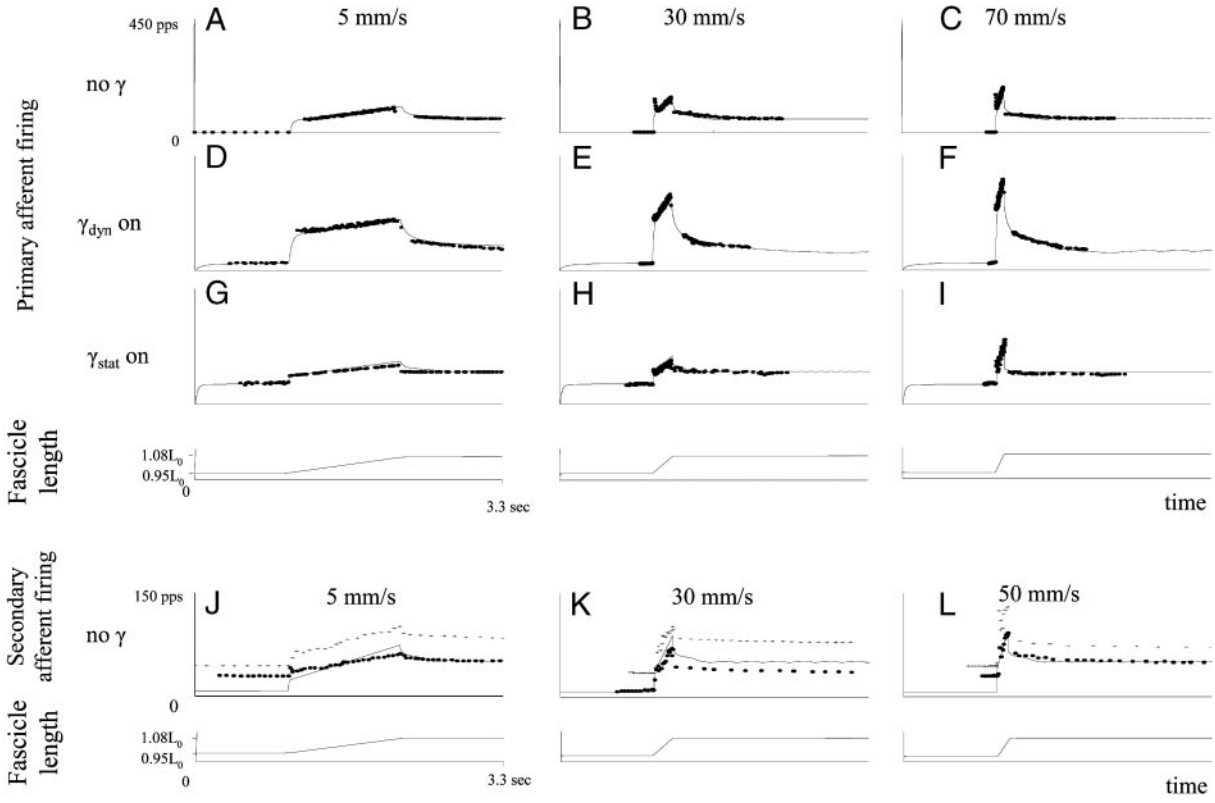

FIG. 3. Spindle model performance during 6-mm whole muscle ramp stretches. Primary afferent response at 3 different velocities (whole muscle stretches at 5, 30, and 70 mm/s; fascicle stretches at 0.11, 0.66, and $1.55L_0$/s; fascicle length changes $0.95–1.08L_0$) were performed in the absence of fusimotor stimulation (*A*, *B*, *C*), during constant dynamic fusimotor stimulation at 70 pps (*D*, *E*, *F*), and during constant static fusimotor stimulation at 70 pps (*G*, *H*, *I*). Solid thin lines represent model output; experimental data are shown as dots (·). Secondary afferent responses at 3 different velocities (whole muscle stretches at 5, 30, and 50 mm/s; fascicle stretches at 0.11, 0.66, and $1.12L_0$/s) are compared with the secondary afferent activity from 2 different muscle spindles (shown as +, ·) originating from the same experimental preparation (*J*, *K*, *L*).

1964; Hulliger et al. 1977a,b; Lennerstrand 1968; Lennerstrand and Thoden 1968a,b; Matthews 1963; Prochazka 1996). Once the selected spindle activity patterns were digitized manually from the figures in the journal articles, MATLAB's Spline Toolbox was used to facilitate parameter optimization, as described below.

The independent data set used for validation of the model originated from the medial gastrocnemius (MG) muscle of the cat rather than the soleus muscle and was similarly digitized manually (Taylor et al. 2000).

An important modification to the above-described data was made to facilitate curve-fitting. The ramp stretch records that were used to develop the model (Crowe and Matthews 1964) were modified in several ways because of their noisiness during the dynamic part of the stretch (which the authors attributed to experimental artifact). This was accomplished by using a cleaner ramp stretch record collected during a single velocity of stretch (Prochazka 1996) and scaling it to match the record recorded by Crowe and Matthew. First we divided Prochazka's afferent record into static and dynamic phases. We assumed that during the stretch the static component increased linearly from initial firing before the stretch to the final level 2–2.5 s after the stretch. The dynamic response was obtained by subtracting this static component from the afferent firing record. Although the static response of Prochazka's data did not require scaling, the dynamic response was scaled to match the dynamic response of afferent activity recorded by Crowe and Matthew. The rest of the data used in tuning and validating the model did not require any such alterations or scaling.

Because the length records from the experiments used in developing the model represent whole muscle length, appropriate calculations were done using an extrafusal model of cat soleus muscle (Brown et al. 1999) to determine the relative contributions of tendon stretch and muscle fascicle (i.e., spindle) length (see APPENDIX 1, *B* and *C*).

FREE PARAMETER OPTIMIZATION. Free parameter optimization was accomplished using the Levenberg–Marquardt optimization method (Press et al. 1986). Data records of ramp, triangular, and sinusoidal stretches in the absence or during constant static and/or dynamic fusimotor stimulation were used to obtain a single set of model parameters for the simulations presented throughout this report.

A single intrafusal fiber model of bag_2 and chain fibers was assumed during this optimization because the bag_2 and chain intrafusal fiber contributions to the activity of the primary afferent could not be quantitatively distinguished during the experiments in which constant fusimotor activity was used. Afterward, the combined bag_2 and chain model was separated based on the simplifying assumption that they share exactly the same structure and parameter values, while having different temporal properties in response to step changes in fusimotor drive (see *Fusimotor activation*). This approach required two parameters relating to static fusimotor stimulation (β_2 and Γ_2) to be scaled to accommodate their different fusimotor saturation points (see Table 1).

Initial parameter optimization runs produced very similar values of K^{SR} and K^{PR} for both the bag_1 and combined bag_2 and chain fibers. We therefore made the simplifying assumption that K^{SR} and K^{PR} were identical for all intrafusal fiber types. Likewise, C_S was found initially to be very similar for the different fiber types and so it, too, was assumed to be a single constant. These simplifying assumptions left ten free parameters as necessary to capture fully the primary afferent

Downloaded from jn.physiology.org on September 18, 2006

activity and two additional parameters to capture secondary afferent activity (Table 1).

In the case of primary afferent parameter optimization, the optimization was broken down into two stages to reduce the number of free parameters optimized simultaneously. The first set of optimizations involved optimization of eight parameters [K^{SR}, K^{PR}, $\beta_0(bag_1)$, $\beta_0(bag_2\&chain)$, $\beta_2(bag_2\&chain)$, $\Gamma_2(bag_2\&chain)$, C_S, L_N^{SR}] for data recorded either in the absence of fusimotor stimulation or during constant static fusimotor stimulation. This was done to introduce just enough dynamic sensitivity into the combined model of the passive bag_2 and chain fibers so that it could be reduced appropriately during the static fusimotor stimulation. Hundreds of optimization runs starting from randomly selected initial points were performed to avoid local minima. After this initial set of optimizations, the parameter values that generated the best fits were used in the next set of optimizations where data involving dynamic fusimotor stimulation were used and two more parameters were optimized [$\beta_1(bag_1)$, $\Gamma_1(bag_1)$]. In addition to using the best-fit parameter values, randomly chosen parameter values in the proximity of the best-fit values were used as well to run a number of optimizations of all ten primary afferent parameters simultaneously (Table 1).

In the case of the secondary afferent model, two additional parameters ("X" and "L_N^{PR}") had to be introduced, explained by the fact that part of the afferent transduction region lies within the polar region of the intrafusal fiber. These two parameters were optimized on the secondary afferent record during 2- and 8-mm/s triangular stretches in the presence of constant static fusimotor stimulation (γ_{static} = 70 pps). The reason for not using other secondary afferent records (5-, 30-, and 50-mm/s ramp stretches and 2- and 8-mm/s triangular stretches in the absence of fusimotor stimulation) is attributed to the existence of several traces of secondary afferent activity during the same kinematic and fusimotor conditions. "L_N^{PR}", the term representing the polar region length above which extension of polar region's secondary afferent endings takes place (see *Eq. 8*), produced the best fit at the value of $0.89L_0$. Interestingly, the parameter "L_N^{PR}", when summed with sensory region rest length ("L_0^{SR}"), resembles approximately the intrafusal fiber length ($0.89L_0 + 0.04L_0 = 0.93L_0$) at which the passive tension develops. Although this value was never previously measured in the case of intrafusal fibers, the extrafusal fiber data indicated that passive tension develops at similar sarcomere lengths (Brown et al. 1996a).

After the parameter optimization, the intrafusal fiber mass (M) was added to individual intrafusal fiber models to increase the model's stability; it had no significant influence on the model's properties.

RESULTS

In the following subsections we show the model's prediction compared with data for each type of movement used in the parameter optimization. This is then followed by validation of the model against novel data that were not used for parameter optimization.

Ramp-and-hold stretches

The model's ability to reproduce primary afferent activity during ramp-and-hold stretches is demonstrated and compared with the experimental data in Fig. 3 (Crowe and Matthews 1964). Whole muscle stretches of 6 mm length (about $0.95L_0$ to $1.08L_0$ fascicle length stretches; see APPENDIX 1, *B* and *C*) at three different velocities (5, 30, and 70 mm/s whole muscle or about 0.11, 0.66, and $1.55L_0$/s fascicle length stretches) were used to run the spindle model simulations in which the fusimotor drive was kept either at zero (Fig. 3, *A*, *B*, and *C*) or at a constant value (Fig. 3, *D*, *E*, and *F*: $\gamma_{dynamic}$ = 70 pps; Fig. 3, *G*, *H*, and *I*: γ_{static} = 70 pps). In the absence of fusimotor stimulation, the model (solid lines) closely agreed with the experimental records of instantaneous primary afferent frequency (dots) for 5 and 30 mm/s, whereas it underestimated the peak dynamic response of the 70-mm/s record by some 20 pps (about 18%). Because the researchers reported having problems with 70-mm/s records and because their published records would suggest an almost linear relationship between dynamic response and velocity that was subsequently refuted (Houk 1981), all 70-mm/s records (with and without any fusimotor stimulation) were excluded from the free parameter optimization. The presence of dynamic fusimotor stimulation during three velocities of stretch increased the dynamic response of the biological spindle, whereas the presence of constant static fusimotor drive had the opposite effect while introducing a strong static bias (Fig. 3, *G*, *H*, and *I*). The primary afferent's dynamic response for 5 and 30 mm/s during static fusimotor stimulation was decreased, whereas the 70-mm/s record remained unaffected. Other published records of primary afferent activity show a consistent decrease in dynamic behavior in response to static fusimotor drive at all velocities, providing further justification to exclude these 70-mm/s records from parameter optimization. Finally, small oscillations in the behavior of the model (e.g., at the end of stretch in Fig. 3, *F* and *H*) were artifacts of the abrupt velocity changes; these can be significantly reduced or eliminated by making such transitions smoother, as they would be in the actual spindle.

Predictions of the secondary afferent model during ramp-and-hold stretches were compared with the secondary afferent data records of two different muscle spindles (Matthews 1963) (Fig. 3, *J*, *K*, and *L*). As seen from the figure, there is great variability in the original data among spindles. Instead of optimizing the X and L_N^{PR} for these records, we used the values (0.7 and $0.89L_0$) that were optimized on the 2- and 8-mm/s triangular stretches in the presence of constant static fusimotor drive where only a single secondary afferent trace existed. In the case of three velocities tested (whole muscle velocities: 5, 30, and 50 mm/s; fascicle velocities: 0.11, 0.66, and $1.12L_0$/s), predictions of the spindle model are contained within the range of the observed variability among secondary afferent firing (see DISCUSSION).

Triangular stretches

The model's ability to capture primary afferent activity during 8-mm whole muscle triangular stretches (fascicle length: $0.90L_0$–$1.08L_0$) at ±8 mm/s (fascicle velocity: $\pm 0.18L_0$/s) was evaluated using data reported by Lennerstrand and Thoden (Lennerstrand 1968; Lennerstrand and Thoden 1968a,b). Lennerstrand and Thoden did not identify from which extensor muscle (soleus or lateral gastrocnemius) the afferent activity originated, but they suggested that the two muscles produced quantitatively similar afferent activity. Triangular stretches in the presence of either dynamic or static fusimotor drives at 35, 70, and 200 pps were available (Fig. 4). The primary afferent model accurately accounted for the spindle's behavior during lengthening (similar to the ramp stretches in Fig. 3), as well as during the shortening case in which the afferent firing was silenced when influenced by dynamic fusimotor stimulation or was maintained when under static fusimotor stimulation. The model performed well during the static

Downloaded from jn.physiology.org on September 18, 2006

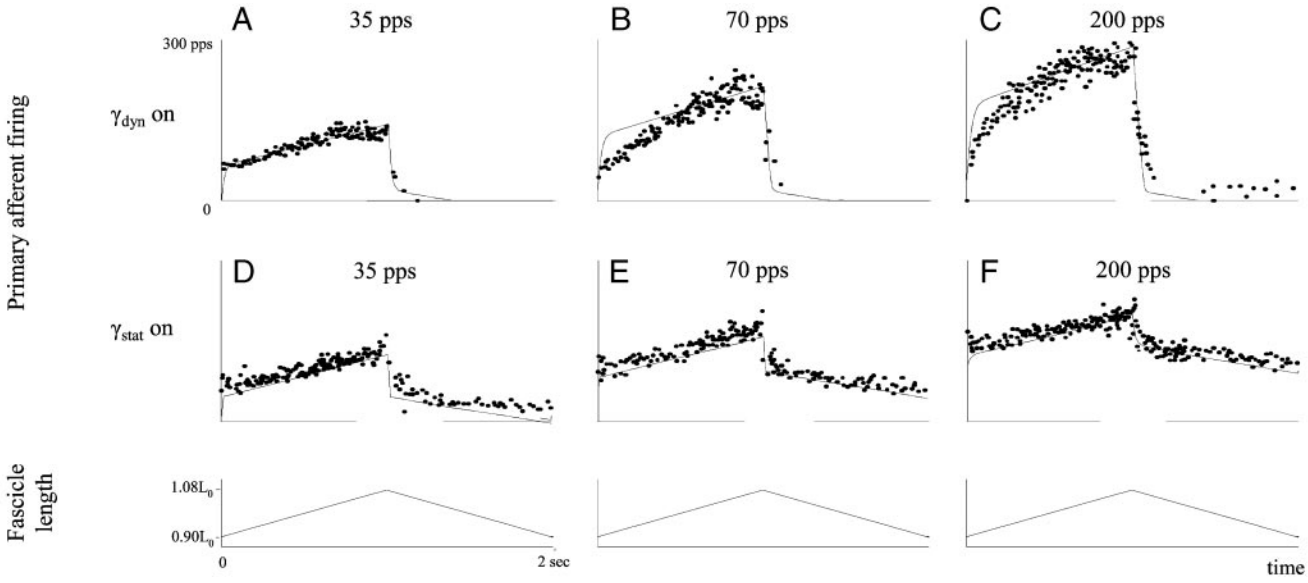

FIG. 4. Model's ability to capture primary afferent activity during triangular stretches. Whole muscle (8 mm) stretches (fascicle length changes 0.90–1.08L_0) at 8 mm/s (fascicle stretches at 0.18L_0/s) were performed during constant dynamic (*A*, *B*, *C*) or static (*D*, *E*, *F*) fusimotor stimulations at 3 different frequencies (35, 70, and 200 pps). Solid thin lines represent model output; experimental data are shown as dots.

fusimotor stimulation. In the case of dynamic fusimotor stimulation, it overestimated the initial dynamic response for the cases of 70- and 200-pps stimulations, and failed to reproduce the recovery of the low-level afferent activity during the second half of shortening in the presence of 200-pps dynamic fusimotor stimulation.

The model's ability to reproduce secondary afferent firing during triangular stretches (Lennerstand and Thoden 1968a,b) is shown in Fig. 5. Whole muscle triangular stretches (2 and 8 mm/s, corresponding to fascicle velocities 0.05L_0/s and 0.18L_0/s) were analyzed in the absence of fusimotor drive (Fig. 5, *A* and *B*), and in the presence of static fusimotor stimulation (Fig. 5, *C* and *D*). The model accurately accounted for the maintained secondary afferent firing during shortening, in contrast to silencing of the primary afferent during this phase of triangular stretch. Because X and L_N^{PR} values were optimized on the triangular stretches in the presence of static fusimotor drive, it is not surprising that the model was very accurate in capturing those records; in the absence of fusimotor stimulation its predictions were contained within the range of the observed variability among secondary afferent firing. Finally, it should be mentioned that this particular set of secondary afferent activity most probably originated from the cat's ankle flexor muscles rather than the extensor muscles (soleus and medial gastrocnemius) that were used in other triangular stretches involving primary afferent activity.

Sinusoidal stretches

Primary afferent activity and the model's performance during whole muscle sinusoidal stretches (1,400 μm peak-to-peak, corresponding to fascicle length 0.995 $\pm$ 0.012L_0) at a frequency of 1 Hz are shown in Fig. 6 (Hulliger et al. 1977a,b). In the first set of experiments, such stretches were applied during constant static or dynamic fusimotor drives with stimulation frequencies of 50, 75, and 125 pps (Fig. 6, *A* and *B*). The published database for sinusoidal stretches also includes simultaneous stimulation of dynamic and static fusimotor efferents. In one set of simulations, dynamic fusimotor drive was held constant at 125 pps, whereas static fusimotor drive was either 50, 75, or 125 pps (Fig. 6*C*) and in the other case static was held at 70 pps, whereas dynamic fusimotor activity was either 50, 75, or 125 pps (Fig. 6*D*).

The records in Fig. 6 are particularly important to demonstrate the effects of occlusion between primary transduction zones. A model with no occlusion (i.e., simple summation) predicts much higher activity in response to combined static and dynamic drive. For example, peak afferent activity during

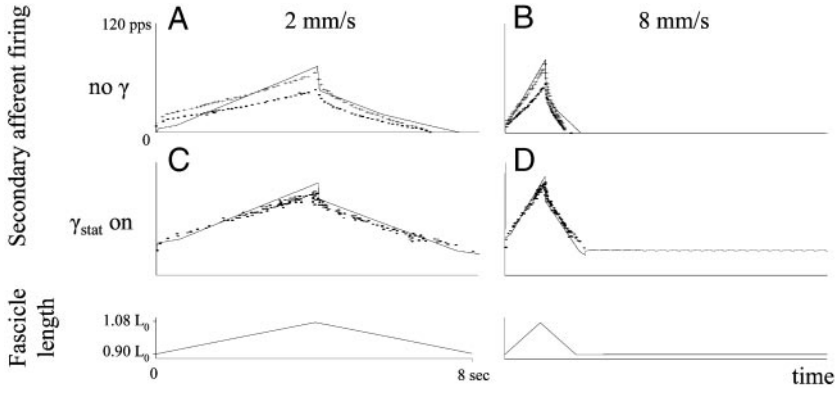

FIG. 5. Model's ability to capture secondary afferent activity during triangular stretches. Whole muscle (8 mm) stretches (fascicle length changes 0.90–1.08L_0) at 2 and 8 mm/s (fascicle stretches at 0.05 and 0.18L_0/s) were performed in the absence of fusimotor stimulation (*A*, *B*) and during static fusimotor stimulation at 70 pps (*C*, *D*). Solid thin lines represent model output; experimental data are shown as dots.

Downloaded from jn.physiology.org on September 18, 2006

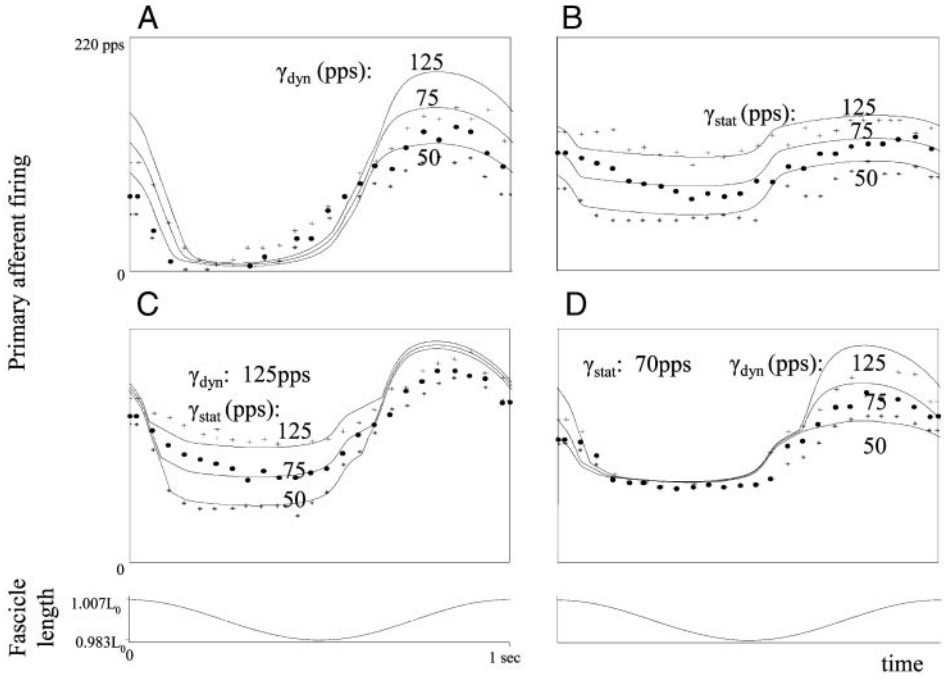

FIG. 6. Model's ability to capture primary afferent activity during sinusoidal stretches and constant fusimotor stimulation. Whole muscle stretches of 1.4 mm peak-to-peak (fascicle length changes 0.995 ± 0.012L_0) at 1 Hz. *A*: dynamic fusimotor stimulation at 50, 75, or 125 pps. *B*: static fusimotor stimulation at 50, 75, or 125 pps. *C*: dynamic fusimotor stimulation at 125 pps plus static fusimotor stimulation at 50, 75, or 125 pps. *D*: static fusimotor stimulation at 70 pps, plus dynamic fusimotor stimulation at 50, 75, or 125 pps. Solid thin lines represent model output; experimental data are shown as +, ·, and *.

stretch with either pure dynamic drive (Fig. 6*A*) or pure static drive (Fig. 6*B*) was around 100 pps; with combined drive at similar rates (Fig. 6, *C* and *D*) it was only slightly higher. A model with complete occlusion (i.e., winner-take-all) would not have demonstrated the complex transition that occurs at the beginning of the stretch phase in the presence of combined static and dynamic drive (Fig. 6, *C* and *D*). Activity during the shortening phase requires static drive because the viscosity of the bag_1 fiber causes its transduction zone to be slack. When the spindle starts to lengthen in the second half of this sinusoidal motion, this same viscosity, amplified by any concurrent dynamic drive, accentuates the stretch of the bag_1 transduction zone, which then modulates but does not yet dominate the activity arising from the bag_2 and chain transduction zones. When stretch velocity peaks, the afferent activity tends to be dominated by the dynamic drive, although residual contributions from different levels of static drive are still apparent. In Fig. 6, *A* and *C*, it is apparent that the model has overestimated the effects of dynamic drive at the highest frequency of 125 pps, perhaps because this particular bag_1 fiber had a somewhat lower saturation frequency than that used in our model (100 Hz). It is important to remember that all of the experimental data from all of the experimental preparations and paradigms in the cited literature were fit with a single set of model parameters.

Model validation

During the early stages of this model's development, the bag_2 and chain fibers were combined into one system because of unavailability of data that would allow quantitative distinction between their properties and because of their similar responses during constant gamma static drive. The bag_2 and chain fibers are distinguished by their different dynamic responses to the onset and offset of fusimotor drive (modeled as low-pass filter intrafusal fiber properties), but these effects had not been studied systematically in recordings of afferent activity during controlled fusimotor stimulation. To test the accuracy of the low-pass filter property of the bag_2 intrafusal fiber included in the model, we used the secondary afferent activity recorded from MG muscle where direct recordings of two types of static fusimotor activity during decerebrate locomotion in the cat and secondary afferent activity were successfully obtained (Taylor et al. 2000). Although the existence of two types of static fusimotor drives is still not universally accepted, the direct fusimotor recordings of Taylor et al. provided convincing new evidence suggesting that type-1 static fusimotor drive innervates chain or bag_2 and chain fibers together, whereas type-2 static fusimotor drive innervates solely the bag_2 fiber.

In the experiments used for our model's validation, Taylor et al. (2000) used a decerebrate cat preparation where locomotor movements of three legs occurred in contact with the treadmill. The experimental leg was denervated except for MG and tibialis anterior (TA) muscles, kept clear of the belt by fixation at midfemur and at the lower end of tibia and allowed to freely rotate about ankle through the phasic contractions of MG and TA. Single-unit recordings were obtained simultaneously from type identified spindle afferents and fusimotor efferents. To reveal the effects of fusimotor drive, Taylor et al. (2000) plotted the secondary difference signal. The secondary difference signal is defined as the difference between the secondary afferent activity recorded during locomotor cycling of the intact MG (where two types of static fusimotor drives were present) and the activity recorded with the leg deefferented (no fusimotor or extrafusal drive), while the ankle was moved through the same trajectory as recorded initially (secondary difference in Fig. 7). We used this experimentally obtained secondary difference signal and compared it to the predicted secondary difference of our model under the same conditions (meaning: secondary activity during same kinematics and simultaneous stimulation of two static fusimotor drives minus the secondary activity during same kinematics and no fusimo-

Downloaded from jn.physiology.org on September 18, 2006

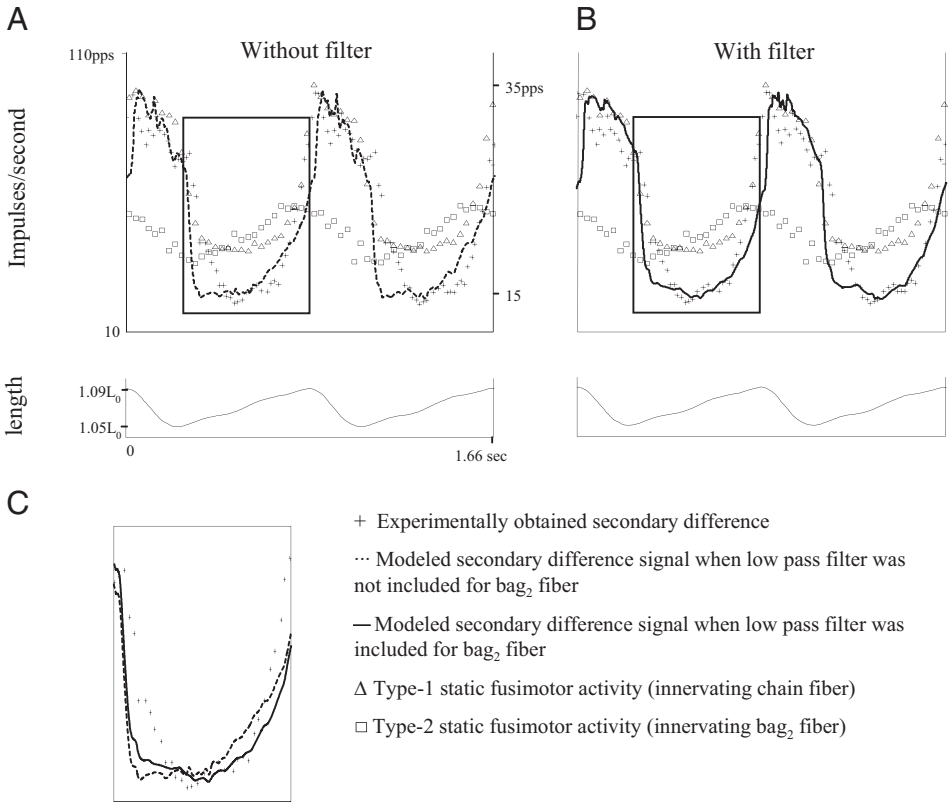

FIG. 7. Model's prediction of the secondary difference signal of secondary afferent during the cat's locomotor step. Secondary difference signal is the difference between the secondary afferent activity recorded during locomotor cycling of the intact MG and the activity recorded with the leg deefferented (no fusimotor or extrafusal drive) while the ankle was moved through the same trajectory as recorded (thin solid lines). In this figure the model's prediction of secondary difference signal during simultaneous stimulation of 2 types of static fusimotor drives [type 1 (△) and type 2 (□), *left* frequency scale] is compared with experimental data (Taylor et al. 2000) (+, *left* frequency scale). Although the amplitude stretch (α) was about 7° of ankle rotation, the mean cycle period lasted for about 0.83 s. Performance of the model lacking low-pass filter property of bag_2 fiber is shown in *A* (thick interrupted line, *right* frequency scale), compared with the performance of the model when low-pass filter was introduced in bag_2 intrafusal fiber model (*B*, thick solid line, *right* frequency scale). *C*: magnified portion of the cycle (enclosed areas in *A* and *B*) where the greatest difference in the performance of the model without and with low-pass filters occurred.

tor drive), both with (Fig. 7*B*) and without (Fig. 7*A*) the inclusion of the low-pass filter for bag_2 intrafusal fiber model (X and L_N^{PR} were set to $0.7L_0$ and $0.89L_0$, respectively).

Based on the ankle angle kinematics provided during decerebrate locomotion it was not possible to calculate the MG fascicle length, but instead a reasonable guess about these values was made. Records suggest that during normal walking, the MG usually operates between the lengths of $0.94L_0$ and $1.14L_0$, which typically corresponds to some 45° of ankle extension (Goslow et al. 1973). Based on the suggested limb's position we assumed that the MG was somewhere in the vicinity of the optimal fascicle length and chose the fascicle length range for the smaller recorded movements to be between $1.05L_0$ and $1.085L_0$ because it produced the best fit for the purpose of modeling the secondary difference signal. Furthermore, a typical spindle contains four to ten chain fibers rather than a single chain fiber (as our model does) which are driven similarly but asynchronously by separate type-1 static fusimotor neurons. Thus our model's secondary difference prediction had to be scaled to fit the experimental data (experimentally obtained secondary difference signal (+ +): *left* frequency scale; modeled secondary difference signal [without low-pass filter (- - -); with low-pass filter (—): *right* frequency scale)]). The inclusion of the low-pass filter in the bag_2 fiber model improved the model's performance (Fig. 7*C*), although a small discrepancy remains at the onset of muscle shortening.

DISCUSSION

Historically the muscle spindle has received much attention because of its importance in sensorimotor control. We chose to build our model of the spindle based on the extensive information available about the internal components and their properties as measured directly in intrafusal fibers, as inferred indirectly from spindle activity during controlled experiments, or as extrapolated from general properties of striated muscle fibers. We are pleased that a single model with one set of coefficients could account for spindle activity from many different preparations under widely varying conditions of motion and fusimotor drive.

Our analysis of the model features and results presented has focused on their ability to capture qualitative behavior rather than quantitative measurements of goodness of fit (e.g., Figs. 6 and 7). Qualitative comparisons are often more instructive than overall quantitative comparisons, which tend to be dominated by portions of the records that happen to have relatively little modulation. Many estimates were required to pool data from various preparations and their disparate descriptions in the literature. Errors in these estimates or heterogeneity in the spindles themselves would be expected to produce offsets in afferent activity levels that would shed little light on the ability of the model to capture the physiological properties of muscle spindles.

An important feature of afferent activity that our model describes accurately is the partial occlusion effect that has been identified in the recent experimental literature (Banks et al. 1997; Carr et al. 1998; Fallon et al. 2001). Modeling of this effect between bag_1 and combined bag_2 and chain intrafusal fiber models reconciled the primary afferent activity during combined static and dynamic fusimotor drive. A somewhat weaker partial occlusion effect has also been reported in the biological spindle during simultaneous stimulation of multiple gamma static motoneurons (Carr et al. 1998; Fallon et al. 2001) but the interpretations of these results are less clear. One suggestion is that the bag_2 fiber drives one impulse generator

Downloaded from jn.physiology.org on September 18, 2006

site, whereas all the other chain fibers (four to 11 of them) collectively drive the other, or that every single chain fiber has a separate impulse-generating site as well. This seems unlikely given their proximity. The nonlinear summation observed during activation of multiple static fusimotor efferents may instead reflect nonlinear summation of the generator potentials themselves. Because of the uncertainty of interpretation of partial occlusion observations during stimulation of multiple static fusimotor efferents and because many researchers still recognize only two impulse-generating sites (one on the bag_1 and the other on the bag_2 and chain fibers), we excluded other occlusion effects in our model.

Our model accounted well for the distinctive activation dynamics of bag_2 versus chain fibers, but there are other differences in the mechanical properties of these intrafusal fibers that were omitted from modeling because of insufficient data. Evidence suggests that the bag_2 fiber is more viscous than the chain fiber [the bag_2 fiber contains slow twitch myosin-ATPase, whereas the chain fiber has the fast twitch form (Ovalle and Smith 1972)], although the afferent records demonstrating this distinction are very noisy. Therefore instead of making arbitrary guesses regarding viscosities of the fibers, we assumed the same viscosities and structures for two intrafusal fiber models but different fusimotor saturation points and temporal properties. Note, however, that the basic structure of the model (Fig. 1) assumes only a single source of static fusimotor drive controlling the bag_2 and chain fibers together, whose composite mechanical properties appear to be well captured by our model.

Our model accounted well for the reported secondary afferent behavior. Because its parameters were optimized on the secondary afferent activity record during two ramp stretches (2 and 8 mm/s) in the presence of static fusimotor activity, it accurately captured those records; in the case where more than a single afferent record was available for the same kinematic and fusimotor conditions, the model predicted the values within the range of observed variability. The reason for the existence of large variability among secondary afferent records is not well understood. Initially we thought that such variability might reflect the variations in the secondary afferent location along different intrafusal fibers. If so, then it could be eliminated by adjusting the X parameter value. However, we realized that this was not sufficient and that it was also necessary to adjust the threshold length of the polar region for transmitting stretch to the secondary ending (L_N^{PR}) to capture the experimental variability. One anatomical feature related to the L_N^{PR} term could be the presence of kinks within the chain fibers, especially in the polar region areas where secondary afferent endings reside (Boyd 1976). A kinked chain fiber might need to be stretched more (i.e., larger L_N^{PR}) and pulled straight before its secondary endings are stretched. To account for variability among individual secondary afferent data, both X and L_N^{PR} parameters probably need to be adjusted.

Finally, it should be mentioned that the model differs from the biological spindle by omitting two effects of movement history: the response to noncycling cross-bridges and the effects of prior movement on the response of the receptors that are unrelated to noncycling cross-bridges (Nichols and Cope 2004). The response to noncycling cross-bridges is believed to give rise to the effect of "stiction" or the initial burst (Proske and Morgan 1999). This mechanism is believed to account for the experimentally observed phenomenon of very high viscosity in the quiescent bag_1 fiber for a very small range of motion, purportedly as a result of the existence of a small number of residual cross-bridges between myofilaments, particularly in the absence of background fusimotor drive (Hill 1968). The consequences of omitting this effect are apparent during very slow and small-amplitude sinusoidal stretches in the absence of fusimotor stimulation, where the model noticeably underestimated the primary afferent activity (not shown), as well as during initial moments of stretch, where an initial burst in afferent firing was not captured by the model (Fig. 3, *B* and *C*). We chose not to model the "stiction" because it seems unlikely to be a factor during most natural motor behavior, in which spindles usually operate over longer stretches and with continuously modulated fusimotor input, both of which eliminate stiction.

Haftel et al. (2004) recently described the phenomena of reduced dynamic response (RDR), in which immediately successive trials of triangular-stretch release produced a systematic reduction in the dynamic response in deefferented spindles in rat triceps surae muscle. In their experiments, the RDR and initial burst properties of the rat's spindle afferents were studied and it was concluded that the initial burst and RDR exhibit very different behavior during successive trials of muscle-stretch release. For example, the initial burst is expressed over a much shorter time and smaller magnitude of muscle stretch than RDR. Additionally, the initial burst recovers more rapidly than RDR and its magnitude is variable and occasionally absent in repeated sets of stretch-release trials, whereas the greater dynamic response is always present in the first trial compared with subsequent trials. At the moment, there are various explanations for the differences between the initial burst and RDR response properties (Haftel et al. 2004). Interestingly, using a similar triangular-stretch–release paradigm in the decerebrate cat where fusimotor activity was present, Houk et al. (1992) found no evidence of change in the dynamic response. If this history-dependent effect occurs only in the absence of fusimotor tone, then its omission should not give rise to significant errors during most conditions of normal use, which typically include substantial fusimotor modulation.

Comparison with previous modeling attempts

Several models of spindle afferent activity have been developed to account for the growing base of physiological data (Chen and Poppele 1978; Crowe 1968, 1970; Hasan 1983; Houk et al. 1981; Lin and Crago 2002; Maltenfort and Burke 2003; Matthews and Stein 1969; Rudjord 1970; Schaafsma et al. 1991). Prochazka and Gorassini (1998) compared the performance of some of these models to experimentally recorded primary and secondary afferent activity from cat hamstring muscles during locomotion. Because the afferent records used for this purpose incorporated intact fusimotor drive and the spindle models did not model these effects, certain assumptions regarding the fusimotor activity had to be made. We chose not to conduct a similar comparison analysis for the purpose of testing the performance of our model because accurate modeling of the fusimotor effects was our major goal. Instead, we chose to concentrate on comparisons only with those models incorporating fusimotor effects (Hasan 1983; Lin

Downloaded from jn.physiology.org on September 18, 2006

and Crago 2002; Maltenfort and Burke 2001; Schaafsma et al. 1991).

Hasan (1983) presented one of the first models consisting of mathematical elements representing the anatomical components found in the biological spindle. The model included a sensory region, which was modeled as a spring, and a polar region, which included nonlinear velocity dependency and a property akin to friction. It addressed issues such as the initial burst response (which we ignored) and fusimotor modulation of afferent activity. Because of both its innovative nature and its easy implementation, Hasan's model attracted the attention of many researchers and its performance has been tested extensively. A major drawback of this model, however, arises from its rigid structure, which requires changing its parameters to account for each fusimotor state. Furthermore, during a series of stretches, the modeled initial burst in afferent activity persists at the start of each stretch, whereas in the biological spindle it is visible only during the first stretch after a period of rest (Matthews 1972).

The next major step in spindle modeling came from Schaafsma et al. (1991), who designed a complex structural model of only the primary afferent that incorporated fusimotor effects. The model consisted of two intrafusal fiber submodels (bag_1 model and combined bag_2 and chain model) and included thixotropic effects, although a mechanism for recovery from these effects was not provided. Subsequently the model was extended to incorporate a simulated chain fiber (Scheepstra et al. 1995). Overall, the model performed well, especially during the ramp-and-hold stretches for which the model parameters were optimized. Limitations in its performance were apparent for sinusoidal stretches (particularly small-amplitude stretches), for which the model underestimated afferent activity. Because the model predates the elucidation of the effect of partial occlusion during simultaneous stimulation of dynamic and static fusimotor efferents (Banks et al. 1997; Carr et al. 1998; Fallon et al. 2001), the model assumes unrealistic, extreme occlusion. In other words, it assumes that the afferent activity will be controlled completely by the larger of the two fusimotor inputs. Although the developers of this model do not report on its performance during conditions of simultaneous static and dynamic fusimotor activation, it is likely that the model would incorrectly predict the afferent firing during those conditions as a consequence of its incorrect occlusion model. Finally, the model does not address the different temporal properties of the three intrafusal fibers.

During the development of the model presented here, two additional spindle models became available (Lin and Crago 2002; Maltenfort and Burke 2001). Maltenfort's spindle model represents a black box model rather than a structural one, whose development was largely inspired by the author's desire to study the effects of β (or also called skeleto-fusimotor) motoneurons, which innervate both intra- and extrafusal muscle fibers (Emonet-Denand and Laporte 1976). Some evidence suggests that β motoneurons receive monosynaptic group Ia excitation comparable to that in α motoneurons, which would then result in a positive feedback loop (Burke and Tsairis 1977). Maltenfort's spindle model is a reasonably simple one and includes the effects of static and dynamic fusimotor activation, as well as the partial occlusion effect. The performance of the model, however, seems to be very limited. For example, during the sinusoidal stretches that were also used in the development of our model (Hulliger et al. 1977a,b), the model's prediction of peak primary afferent firing in the presence of dynamic fusimotor stimulation (either when present alone or in combination with static fusimotor stimulation; see Fig. 6, *A*, *C*, and *D*) was on average 70 pps larger than in the biological spindle. Maltenfort's model also underrepresents the decreased modulation of primary afferent firing during increasing static fusimotor stimulation (8–24 pps in their model vs. 25–45 pps in the biological spindle; our model's performance during identical circumstances is shown in Fig. 6*B*). Finally, their model contains no terms that would enable it to capture the response times of individual intrafusal fibers when subject to modulated fusimotor activity.

About the same time that Maltenfort's black box model appeared in the literature, Lin and Crago (2002) presented a combined model of extrafusal muscle and spindle, to study how the spindle is related to the extrafusal muscle and how it operates internally. A Hill-type muscle model represented the extrafusal muscle fibers, whereas the spindle model was a structural one consisting of three intrafusal fiber models. Overall, 89 parameters, out of which 24 were free parameters, were used in this model. Lin and Crago's model calculates the intrafusal muscle force by multiplication of the activation level times the output of the force–length curve times the output of the force–velocity curve, similarly to extrafusal fibers. A similar relationship is also embedded in our model where the force within the polar region results partially from the multiplicative relationship between forces ascribed to length and velocity and activation $[B \times C \times (L^{PR} - R) \times \text{sign}\, L^{\bullet PR}) \times \text{abs}\, (L^{\bullet PR})^a]$.

Lin and Crago assumed that each intrafusal fiber acts as an independent impulse generator, despite the widely accepted notion that there are only two impulse-generating sites (Banks et al. 1997; Carr et al. 1998; Celichowski et al. 1994; Fallon et al. 2001). The primary afferent was modeled as resulting from the complete, rather than the partial, occlusion between the bag_1 and bag_2 fiber activities (rather than from the activities in all three intrafusal fibers as in the biological spindle). Similarly, the secondary afferent activity resulted from complete occlusion among the activities in bag_2 and chain fibers. In the case of the primary afferent, the model performed well during ramp-and-hold and sinusoidal stretches, especially during the stimulation of individual fusimotor inputs, while demonstrating certain limitations in the absence of such inputs. In the case of the ramp-and-hold stretch, the model underestimates the afferent decay time after completion of the stretch, especially in the absence of any fusimotor stimulation (0.2 vs. 0.5 s). Also, at the completion of the stretching phase of a ramp-and-hold stretch, the model predicts an abrupt and brief cessation of firing, which might be a troubling artifact if the model is to be incorporated into a model of segmental regulation of motor output, as intended by the authors.

Lin and Crago did not describe the performance of their model during combined fusimotor stimulation, except for a single ramp-and-hold example presented without matching experimental data. Because the model uses complete rather than partial occlusion, it seems likely that the model will underestimate afferent activity during conditions of simultaneous fusimotor stimulation. For purposes of modeling the secondary afferents, the chain fiber was modeled separately, although as the authors mention, the separation between the bag_2 and chain fibers was based on qualitative rather than

Downloaded from jn.physiology.org on September 18, 2006

quantitative observations because of insufficient experimental data (fusimotor stimulation of the chain fiber increases the static sensitivity and the baseline firing, whereas stimulation of bag_2 had no or only a slight effect on static sensitivity; Boyd 1981). The benefit of a complete set of free parameters for each of the two fiber types (rather than modeling them as one fiber type with different dynamics) is not clear, especially if only a single source of static fusimotor drive is available. Furthermore, it should be mentioned that the model assumes that the secondary afferent endings span exactly the same region on the bag_2 and chain intrafusal fibers as the primary endings occupy (the sensory region), despite the fact that in the biological spindle the secondary endings are located on more juxtaequatorial regions of intrafusal fibers that exhibit some polar region properties. Although this simplification might be acceptable during muscle lengthening where the primary and secondary afferents behave similarly, it is likely to introduce errors during shortening where very different behaviors have been observed in primary and secondary afferents (especially during low or absent static fusimotor stimulation, when the primary afferent becomes silent, whereas the secondary afferent continues to fire).

Lin and Crago's model includes individual intrafusal fiber time constants of activation dynamics (low-pass filter properties). Although the chain fiber's time constant seems appropriate (0.08 s), the values for bag_1 and bag_2 fibers appear to be too short (0.16 and 0.24 s, respectively) compared with the experimental measurements [bag_1: 0.82 s (Boyd 1976) and 1.24 s (Boyd et al. 1977); bag_2: 0.53 s (Boyd 1976) and 0.70 s (Boyd et al. 1977)]. It is surprising that the bag_1 was modeled as having a shorter time constant than that of the bag_2 fiber because the two fibers were traditionally called slow and fast nuclear bag fibers, respectively (Boyd 1976).

The role of the spindle model in understanding the fusimotor system

The exact pattern and purpose of fusimotor activity during natural motor behavior remain controversial. One general proposal is that the spindle is thereby programmed by the CNS so as to behave as an optimal transducer (Loeb 1984; Loeb and Marks 1985; Scott and Loeb 1994). The information-transmitting capability of a given spindle afferent is limited by the physiological range of firing rates and noisiness in the interval between successive action potentials, particularly when asynchronous signals from multiple afferents are combined (Loeb and Marks 1985). If the spindle had a fixed sensitivity to length and velocity, it would be incapable of distinguishing fine gradations of the wide range of lengths and velocities over which muscles can operate. The CNS can improve utility of the spindle afferent signal by adjusting its sensitivity in consideration of the relatively limited range of lengths and velocities that it expects to encounter during a self-generated behavior (e.g., locomotion). In the following paragraphs we will discuss the current understanding of fusimotor control and the role it plays during natural locomotion. In doing so, we will point out some examples where our spindle model could help to resolve uncertainties regarding the nature and effects of fusimotor control.

Natural patterns of fusimotor activity

Recordings of fusimotor activity during locomotor behavior are scarce because of the difficulty of the experiment. A few direct recordings have been reported from reduced preparations, but it was problematic to identify the source as being static or dynamic (Appenteng et al. 1980; Lund et al. 1979; Murphy et al. 1984). Recordings of primary afferent activity during locomotion are more common, so investigators often attempt to infer fusimotor programming by comparing the afferent firing rates to those that would have been expected in the absence of fusimotor activity.

Recently, the records of fusimotor efferent firing in medial gastrocnemius muscle (MG) during decerebrate locomotion of the cat were successfully captured, providing more direct insight into fusimotor function (Taylor et al. 2000). The dynamic fusimotor efferent increased its activity abruptly at the beginning of active shortening of MG, stayed constant during that phase, and became silent at the beginning of its stretch by the antagonist dorsiflexors of the ankle. The authors hypothesized that the increased dynamic fusimotor stimulation during the shortening phase would enhance detection and reflex effects of any unexpected lengthening that might result from obstruction of the limb's trajectory. Furthermore, the residual dynamic fusimotor effects during the initial moments of lengthening resulted in a large burst in primary afferent firing, which was hypothesized to represent a cue signal to CNS indicating the beginning of the swing phase. When making such an interpretations, however, it should be remembered that the kinematics of the muscles in Taylor et al.'s unloaded decerebrate preparation were quite unlike those of normal locomotion; the decerebrate CNS presumably has no way of adapting fusimotor control for such altered and unexpected changes in kinematics. It should be possible to drive our model with the kinematics of normally loaded walking plus the fusimotor activity recorded from unloaded, decerebrate preparation to see whether it produces spindle afferent activity patterns consistent with those recorded from intact, naturally walking animals.

In addition to capturing the dynamic fusimotor pattern during natural locomotor step, Taylor et al. recorded static fusimotor activity as well. The static fusimotor activity was found to be strongest during the periods of active shortening of MG in decerebrate locomotion. This was found to introduce a strong bias to the afferent firing, preventing it from going silent. Although the existence of two types of static fusimotor drives is still not widely accepted, the direct fusimotor recordings provided convincing new evidence for this (Taylor et al. 2000). During the locomotor step the two efferent firing profiles were somewhat out of phase; type 2 drive (presumed to be innervating bag_2 fiber) lead the type 1 drive (innervating chain fibers) by about 0.17 s. These phase differences appear to compensate for the differences in contractile dynamics of their respective intrafusal fibers (see APPENDIX 1; Boyd 1976; Boyd et al. 1977), resulting in synchronous static fusimotor modulation of the receptors. Thus it remains unclear whether these two types of static fusimotor modulation are actually used differentially in some behaviors.

Finally, one very useful function of our model that is currently being investigated deals with inverting the model, so that the available records of the spindle's afferent activity and

Downloaded from jn.physiology.org on September 18, 2006

the muscle length changes during natural locomotion could be used to calculate the underlying fusimotor pattern that gave rise to the recorded afferent activity. Even though the inversion of the secondary afferent model was straightforward, the existence of nonlinear partial occlusion term made the inversion more complicated in the case of the primary afferent. The recently available direct recordings of fusimotor activity in the decerebrate cat (Taylor et al. 2000) allowed us to make some useful assumptions while inverting the primary afferent; the bag_2 and chain intrafusal fibers were assumed to represent a dominant pacemaker site during muscle shortening, whereas the bag_1 was assumed to be the dominant site during muscle lengthening. Preliminary results agreed qualitatively with Taylor's conclusions regarding fusimotor activity during decerebrate cat locomotion, but they also revealed the importance of having accurate kinematic records. For the older experimental recordings that we used (Loeb and Duysens 1979; Loeb and Hoffer 1985; Loeb et al. 1985), the muscle velocity and length records were often extrapolated from synergistic or antagonistic muscles with different musculoskeletal architecture from the source of the spindle afferent recordings. The inverted spindle model was extremely sensitive to minor misalignment between the afferent record and muscle kinematics because it compensated for any discrepancy by using the fusimotor apparatus.

In conclusion, we are encouraged that a single set of model parameter values accurately captured the behavior of spindle afferents from different experimental preparations under widely varying kinematic and fusimotor conditions, including a complex data set not included in the optimization of any of the parameters. This provides indirect support for unifying hypotheses regarding the function of fusimotor control and the contribution of information from spindle afferents to kinesthesia and sensorimotor control in general. Although the number of parameters that had to be specified is fairly large, the anatomically based design of the model facilitated a bootstrapping approach in which some individual parameters could be set directly from literature values or from specific experiments designed to reveal a particular property of a given spindle structure. The correspondence between model terms and anatomical components facilitates the formulation and experimental testing of specific hypotheses about transduction in spindles such as those related to occlusion and phasing.

The model itself will be useful in several ways. Most directly, it can be used to demonstrate the effects of particular patterns of fusimotor activity on the sensitivity of spindle afferents to a given set of kinematic inputs. Conversely, it can be inverted to infer fusimotor activity from patterns of activity in spindle afferents, which are relatively easy to record in both reduced and naturally behaving preparations. More generally, realistic representations of spindle afferent activity in larger models of neural control systems will provide better understanding of the actual control problems that must be solved by those systems. Currently, the model has been successfully incorporated into a relatively complex model of the human arm with 15 muscles (Lan et al. 2005). One key feature of the model is that it can be implemented in a Simulink block defined by a MATLAB S-function, and seamlessly incorporated into the Virtual Muscle model (Cheng 2000), or any other muscle model defined with a Simulink block.

APPENDIX 1

A: Designing the low-pass filters

DETERMINING THE CONTRACTILE DYNAMICS OF INDIVIDUAL INTRAFUSAL FIBER TYPES IN THE PRESENCE OF MODULATED FUSIMOTOR ACTIVATION. The primary data for the time constants of individual intrafusal fiber contractions during fusimotor stimulation are from Boyd (Boyd 1976; Boyd et al. 1977). In the first set of such experiments (Boyd 1976) the spindles from tenuissimus muscle of the cat were successfully isolated with most or all of their innervation intact. Their intrafusal fiber contraction and relaxation properties were observed and recorded on still or moving film. The individual fusimotor axons to the spindle were not isolated, but instead the stimulus to the nerve was gradually increased, activating multiple fusimotor efferents and resulting in the multiple intrafusal fiber contractions. Therefore the individual intrafusal fiber measurements were performed at the same time when most other intrafusal fibers were contracting in the spindle, which probably reflects normal fusimotor patterns of activity. The mean times of the complete contraction for individual bag_1 and bag_2 fibers and the chain bundle (rather than a single chain fiber) were 0.82, 0.53, and 0.48 s, respectively. In the second set of experiments (Boyd et al. 1977) the individual fusimotor efferents to the spindles were isolated and their connections to particular intrafusal fibers identified. Dynamic fusimotor efferents were related to bag_1 intrafusal fibers, whereas static fusimotor efferents were identified as being selective and innervating either bag_2 or chain fibers, or as being nonselective and innervating both fibers. By appropriately stimulating individual intrafusal fibers, the mean times of the complete contraction for individual bag_1 and bag_2 fibers and bundle of chain fibers were measured to be 1.24, 0.70, and 0.35 s, respectively. The two experiments (Boyd 1976; Boyd et al. 1977) agree that the bag_1 fiber has the longest contraction time among the intrafusal fibers. In the case of bag_2 and chain fibers, the first experiment suggests that their time constants are similar, whereas the second one describes a significantly slower nature of bag_2 fiber compared with the chain fiber.

Inspired by the recent primary afferent recordings during sinusoidally modulated fusimotor efferent stimulation (1 Hz, 50 ± 30 pps) of individual intrafusal fibers, we took a closer look at their implications regarding individual fiber contraction times (Durbaba et al. 2001). The recorded data suggest that chain fibers respond to static fusimotor stimulation with little or no delay (Durbaba et al. 2001: primary gain 0.25, primary phase lag 3°), which seems surprisingly low compared with Boyd's complete contraction times of 0.48 (Boyd 1976) and 0.35 s (Boyd et al. 1977) in response to sustained static fusimotor stimulation. In the light of these new observations, we returned to Boyd's experiments to search for experimental conditions that might have resulted in longer chain contraction times. We found that in most of the spindles, Boyd identified and stimulated only a single static fusimotor efferent innervating the chain fibers and assumed that it was innervating the entire chain bundle. The experimental evidence, however, suggests that a single static fusimotor efferent innervates either one or two chain fibers, and only rarely three fibers, whereas a single spindle on average has between four and 11 chain fibers (Boyd and Ward 1975). During stimulation of a single static fusimotor efferent, the bundle of chain fibers in the spindle tends to respond as a single unit, possibly because passive chain fibers are bound to active ones by connective tissue (Boyd and Ward 1975). In light of Boyd's comment on the difficulty of clearly observing the chain contraction pattern arising from the fibers' small diameters and close packing, we argue that the Boyd's unexpectedly long contraction time might be the result of incomplete fusimotor stimulation of the chain bundle. Activation of only a few of the chain fibers could have significantly slowed the overall contraction of the bundle. Therefore we decided to use the recently obtained observations that suggest almost zero contraction time for chain fibers (Durbaba et al. 2001). These are consistent with the well-known ability of static fusimotor efferents to entrain spindle

Downloaded from jn.physiology.org on September 18, 2006

afferent activity at rates of 50–100 pps when stimulated individually (Boyd 1986).

Bag_1 and bag_2 fibers have simpler fusimotor innervation than the set of chain fibers, so Boyd's measured complete contraction time constants are more likely to be accurate (bag_1: 1.24 s; bag_2: 0.70 s; Boyd 1977). Nevertheless, we again looked at the recently obtained records of the primary afferent firing when individual intrafusal fibers were sinusoidally stimulated (γ_{static}: 1 Hz, 50 ± 30 pps) as described earlier (Durbaba et al. 2001). The primary afferent data suggest that the bag_2 fiber cannot significantly modulate afferent activity at even this low modulation frequency (primary gain: 0.1; Durbaba et al. 2001). Nevertheless, the researchers decided to fit the afferent activity with a sinusoidal curve to calculate its phase lag compared with the sinusoidal static fusimotor stimulation (primary phase lag: 53° or 0.15 s). The problem is compounded by the fact that much of the high range of the FM occurred at stimulation frequencies for which bag_2 activation saturates (60–75 pps). Instead, we decided to look at the lower half of the sinusoidal curve (i.e., where static fusimotor frequencies were between 20 and 50 pps) to examine the modulation gain and phase lag values for the bag_2 fiber. Even there, we found very little afferent modulation. In Boyd's earlier work, a ramp increase in static fusimotor stimulation to the bag_2 significantly altered the afferent firing (i.e., the increase in the static fusimotor activation of the bag_2 fiber from 30 to 60 pps resulted in an increase of about 30 pps in the primary afferent firing; Boyd 1986). All of these data are consistent with the contraction time of 0.70 s measured by Boyd et al. (1977) and used in designing of our low-pass filter for type 2 static innervation of the bag_2 fiber. Very similar observations were also obtained for the bag_1 fiber, which was found to be incapable of modulating the primary afferent activity during sinusoidal dynamic fusimotor stimulation at 1 Hz (Durbaba et al. 2001). Therefore Boyd's measured complete contraction time constant was used in developing the bag_1 low-pass filter (1.24 s; Boyd et al. 1977). In designing the bag_1 and bag_2 fiber low-pass filters we chose contraction time measurements from individual intrafusal fibers (Boyd et al. 1977), rather than during simultaneous contraction of multiple intrafusal fibers (Boyd 1976), because the onset of fusimotor activation of each intrafusal fiber in the later experiments was not known, so time constants had to be estimated subjectively.

DETERMINING TIME CONSTANTS FOR LOW-PASS FILTERS. Initially, very high fusimotor frequencies (bag_1 and bag_2: 100 Hz; chain: 150 Hz) were applied to each intrafusal fiber model to measure the time it takes each intrafusal fiber model to contract to nearly 90% of the maximum (bag_1: 0.5 s; bag_2: 0.005 s; chain: 0.005 s). For bag_1 and bag_2 intrafusal fiber models, these 90% contraction times were shorter than the 90% contraction values that we estimated from biological intrafusal fibers (bag_1: 0.843 s; bag_2: 0.476 s; Boyd et al. 1977) based on similar estimates in an earlier work (Boyd 1976). To reconcile these differences, we assumed a low-pass filter behavior for bag_1 and bag_2 fibers and designed appropriate filters for the two fibers

$$f_{dynamic}(t) = [1 - e^{-(t/\tau)}] \times \frac{\gamma^P_{dynamic}}{\gamma^P_{dynamic} + freq^P_{bag_1}} \quad \text{(bag 1)}$$

$$f_{static}(t) = [1 - e^{-(t/\tau)}] \times \frac{\gamma^P_{static}}{\gamma^P_{static} + freq^P_{bag_2}} \quad \text{(bag 2)}$$

For each intrafusal fiber, the constant (τ) was calculated by setting:

- $f_{dynamic} = 0.9 \times 0.735$ (for bag_1 case) or $f_{static} = 0.9 \times 0.735$ (for bag_2 case) because the rise times to nearly 90% of the intrafusal fiber contraction during 100-Hz frequency were measured (note that $f_{dynamic} = 0.735$ for bag_1 fiber at 100 Hz and $f_{static} = 0.735$ for bag_2 fiber at 100 Hz), and
- $\gamma^P_{dynamic}/(\gamma^P_{dynamic} + freq^P_{bag1}) = 0.735$ (for bag_1 case) or $\gamma^P_{static}/(\gamma^P_{static} + freq^P_{bag2}) = 0.735$ (for bag_2 case) because 100-Hz fusimotor stimulations were used;
- time t was equal to the difference in 90% contraction rise times between biological intrafusal fiber and intrafusal fiber model (bag_1: 0.843 s − 0.500 s = 0.343 s; bag_2: 0.476 s − 0.005 s = 0.471 s).

The calculated values of constant τ were 0.149 and 0.205 for bag_1 and bag_2, respectively.

B: Calculating the maximal fascicle length from the whole muscle length during passive stretch

To calculate the maximal muscle fascicle length during passive stretch (L^f_{max}), maximal whole muscle length (L^{MT}_{max}), and tendon and aponeurosis length during maximal passive stretch ($L^T_{max\ passive}$) must be determined.

1. CALCULATION OF THE MAXIMAL WHOLE MUSCLE LENGTH (L^{MT}_{MAX}). The values used in these calculations were based on the measurements of soleus muscle made by Scott et al. (1996):

- Optimal muscle fiber fascicle length (L^f_0) = 3.8 cm
- Length of whole-muscle at L_0 (L^{MT}_0) = 10.9 cm
- Range of motion (ROM) = 2.5 cm
- L_0 relative to ROM (% from shortest length) = 85%

L^{MT}_{max} is then calculated

$$L^{MT}_{max} = L^{MT}_0 + (1 - 0.85) \times ROM = 11.275 \text{ cm}$$

2. CALCULATION OF TENDON AND APONEUROSIS LENGTH DURING MAXIMAL PASSIVE STRETCH ($L^T_{max\ passive}$). In determining this value we used soleus data where the measurements of force produced by the muscle (in units of F_0, where F_0 represents muscle force at optimal fascicle length L_0) were compared with the measured length of the tendon and aponeurosis (in units of L^T_0, where L^T_0 represents optimal tendon and aponeurosis length at F_0) (Brown et al. 1996b). We first determined the passive stress produced by the muscle when stretched to the maximal physiological length to be 4 N/cm^2 (Brown et al. 1996a), which was then normalized by F_0/PCSA (32 N/cm^2; Scott et al. 1996) to get this value in units of F_0 [(4 N/cm^2)/(32 N/cm^2) = $0.125F_0$]. The length of tendon and aponeurosis at force $0.125F_0$ was approximated to the value $0.96L^T_0$ (Brown et al. 1996b). To obtain this value in centimeters, L^T_0 was estimated based on tendon slack length [L^T_{slack} = 7.1 cm (Scott et al. 1996); $L^T_{slack} = 0.94 \times L^T_0$; $L^T_0 = (1/0.94) \times L^T_{slack}$ = 7.553 cm] and the tendon and aponeurosis length during maximal passive stretch was: $L^T_{max\ passive} = 0.96 \times 7.553$ cm = 7.251 cm.

3. CALCULATION OF THE MAXIMAL MUSCLE FASCICLE LENGTH (L^F_{MAX}) DURING PASSIVE STRETCH. The maximal fascicle length was determined by subtracting $L_{max\ passive}$ from L^{MT}_{max}

$$L^f_{max} = L^{MT}_{max} - L^T_{max\ passive} = 11.275 - 7.251 = 4.024 \text{ cm}$$

C: Calculation of the amount of muscle fascicle stretch from the whole muscle stretch

In the following calculations the equations of the model describing properties of the mammalian skeletal muscle (soleus) were used (Brown et al. 1999) to determine muscle fascicle stretch. Under passive conditions, the whole muscle model consists of two nonlinear springs in series: the parallel elastic (PE) element (which lies in parallel with the contractile element) and the series elastic (SE) element representing the tendon and aponeurosis. During the passive stretch, the force produced in the active contractile element is zero and the force in the nonlinear spring is

Downloaded from jn.physiology.org on September 18, 2006

$$F_{PE} = c_1 \times k_1 \times \ln\left[\exp\left(\frac{L^f - L_{r1}}{k_1}\right) + 1\right]$$

where c_1, k_1, and L_{r1} are measured constants for soleus muscle ($c_1 = 76.4$, $k_1 = 0.053$, $L_{r1} = 1.4$) and L^f is the fascicle length in units of L_0. By inverting this equation, an equation for fascicle length can be obtained

$$L^f = k_1 \times \ln\left[\exp\left(\frac{F_{PE}}{c_1 \times k_1}\right) - 1\right] + L_{r1}$$

The force in the tendon and aponeurosis is equal to

$$F_{SE} = c^T \times k^T \times \ln\left[\exp\left(\frac{L^T - L_r^T}{k^T}\right) + 1\right]$$

where c^T, k^T, and L_r^T are measured constants for soleus muscle ($c^T = 27.8$, $k^T = 0.0047$, $L_r^T = 0.964$) and L^T is tendon length in units of L_0^T.

Because the force in the fascicle area is equal to the force in the tendon and aponeurosis area ($F_{PE} = F_{SE}$), the equation for F_{SE} can be used and substituted in the previous equation for L^f

$$L^f = k_1 \times \ln\left\langle \exp\left\{\frac{c^T \times k^T \times \ln\left[\exp\left(\frac{L_T - L_r^T}{k^T}\right) + 1\right]}{c_1 \times k_1}\right\} - 1\right\rangle + L_{r1}$$

Because the experimental literature dealing with spindle activity provides the whole muscle length, the tendon length in the previous equation can be expressed in terms of fascicle length and whole muscle length

$$L_T = \frac{L^{WM} - L_0^f \times L^f}{L_0^T}$$

Therefore we are left with the following equation, which needs to be solved for L_f

$$L^f = k_1 \times \ln\left\langle \exp\left\{\frac{c^T \times k^T \times \ln\left[\exp\left(\frac{\frac{L^{WM} - L_0^f \times L^f}{L_0^T} - L_r^T}{k^T}\right) + 1\right]}{c_1 \times k_1}\right\} - 1\right\rangle + L_{r1}$$

An analytical solution of this equation in terms of constants does not exist. Instead, values of constants and whole muscle length as described above were provided to MATLAB to calculate the fascicle length L_f.

ACKNOWLEDGMENTS

The authors thank Dr. Rade Durbaba for providing data and comments pertinent to those data.

REFERENCES

Appenteng K, Morimoto T, and Taylor A. Fusimotor activity in masseter nerve of the cat during reflex movements. *J Physiol* 350: 415–431, 1980.

Bakker GJ. *Histochemical Characteristics of Muscle Spindle in Cat Dorsal Neck Muscles* (MS thesis). Kingston, Ontario, Canada: Queen's Univ. Press, 1980.

Banks RW. The motor innervation of mammalian muscle spindles. *Prog Neurobiol* 43: 323–362, 1994.

Banks RW, Hulliger M, Scheepstra KA, and Otten E. Pacemaker activity in a sensory ending with multiple encoding sites: the cat muscle spindle primary ending. *J Physiol* 498: 177–199, 1997.

Barker D. The structure and distribution of muscle receptors. In: *Symposium on Muscle Receptors*, edited by Barker D. Hong Kong: Hong Kong Univ. Press, 1962, p. 227–240.

Barker D. The morphology of muscle receptors. In: *Handbook of Sensory Physiology*, edited by Hunt CC. Berlin: Springer-Verlag, 1974, vol. 3, pt. 2, p. 1–190.

Bessou P and Pages B. Cinematographic analysis of contractile events produced in intrafusal muscle fibers by stimulation of static and dynamic fusimotor axons. *J Physiol* 252: 397–427, 1975.

Boyd IA. The response of fast and slow nuclear bag fibers in isolated cat muscle spindles to fusimotor stimulation, and the effect of intrafusal contraction on the sensory endings. *Q J Exp Physiol* 61: 203–254, 1976.

Boyd IA. The action of the three types of intrafusal fiber in isolated cat muscle spindles of the dynamic and length sensitivities of primary and secondary sensory endings. In: *Muscle Receptors and Movement*, edited by Taylor A and Prochazka A. London: Macmillan, 1981.

Boyd IA. Two types of static γ-axons in cat muscle spindles. *Q J Exp Physiol* 71: 307–327, 1986.

Boyd IA, Gladden MH, McWilliam PN, and Ward J. Control of dynamic and static nuclear nag fibers and nuclear chain fibers by gamma and beta axons in isolated cat muscle spindles. *J Physiol* 265: 133–162, 1977.

Boyd IA and Smith R. The muscle spindle. In: *Peripheral Neuropathy*, edited by Dyck PJ, Thomas PK, Lombert EH, and Bunger R. Philadelphia, PA: Saunders, 1984, p. 171–202.

Boyd IA and Ward J. Motor control of nuclear bag and nuclear chain intrafusal fibers in isolated living muscle spindles from the cat. *J Physiol* 244: 83–112, 1975.

Brown IE, Cheng EJ, and Loeb GE. Measured and modeled properties of mammalian skeletal muscle. II. The effects of stimulus frequency and force–length and force–velocity relationships. *J Muscle Res Cell Motil* 20: 627–643, 1999.

Brown IE, Liinamaa TL, and Loeb GE. Relationship between range of motion, L_0, and passive force in five strap-like muscles of the feline hindlimb. *J Morphol* 230: 69–77, 1996a.

Brown IE and Loeb GE. Measured and modeled properties of mammalian skeletal muscle. IV. Dynamics of activation and deactivation. *J Muscle Res Cell Motil* 21: 33–47, 2000.

Brown IE, Scott SH, and Loeb GE. Mechanics of feline soleus. II. Design and validation of mathematical model. *J Muscle Res Cell Motil* 17: 221–233, 1996b.

Burke RE and Tsairis P. Histochemical and physiological profile of a skeletofusimotor (β) unit in cat soleus muscle. *Brain Res* 129: 341–345, 1977.

Carr RW, Gregory JE, and Proske U. Summation of responses of cat muscle spindles to combined static and dynamic fusimotor stimulation. *Brain Res* 800: 97–104, 1998.

Celichowski J, Emonet-Denand F, Laporte Y, and Petit J. Distribution of static γ axons in cat peroneus tertius spindles determined by exclusively physiological criteria. *J Neurophysiol* 71: 722–732, 1994.

Chen WJ and Poppele RE. Small-signal analysis of response of mammalian muscle spindles with fusimotor stimulation and a comparison with large-signal properties. *J Neurophysiol* 41: 15–27, 1978.

Cheng EJ, Brown IE, and Loeb GE. Virtual muscle: a computational approach to understanding the effects of muscle properties on motor control. *J Neurosci Methods* 101: 117–130, 2000.

Crowe A. A mechanical model of the mammalian muscle spindle. *J Theor Biol* 21: 21–41, 1968.

Crowe A. A mechanical model of muscle and its application to the intrafusal fibers of the mammalian muscle spindle. *J Biomech* 3: 583–592, 1970.

Crowe A and Matthews PBC. The effects of stimulation of static and dynamic fusimotor fibers on the response to stretching of the primary endings of muscle spindles. *J Physiol* 174: 109–131, 1964.

Durbaba R, Taylor A, Elleway PH, and Rawlinson S. Modulation of primary afferent discharge by dynamic and static gamma motor axons in cat muscle spindles in relation to the intrafusal fibre types activated. *J Physiol* 532: 563–574, 2001.

Eldred E, Bridgman CF, Sweet JE, and Eldred B. Quantitative comparisons of muscle receptors of the cat medial gastrocnemius, soleus and extensor digitorum brevis muscles. In: *Symposium on Muscle Receptors*, edited by Barker D. Hong Kong: Hong Kong Univ. Press, 1962, p. 207–213.

Emonet-Denand F and Laporte Y. The skeleto-fusimotor innervation of cat muscle spindle. *Prog Brain Res* 44: 99–109, 1976.

Downloaded from jn.physiology.org on September 18, 2006

Fallon JB, Carr RW, Gregory JE, and Proske U. Summing responses of cat soleus muscle spindles to combined static and dynamic fusimotor stimulation. *Brain Res* 888: 348–355, 2001.

Goslow GE, Reinking RM, and Stuart DS. The cat step cycle: hind limb joint angles and muscle lengths during unrestrained locomotion. *J Morphol* 141: 1–42, 1973.

Haftel VK, Bichler EK, Nichols TR, Pinter MJ, and Cope TC. Movement reduces the dynamic response of muscle spindle afferents and motoneuron synaptic potentials in rat. *J Neurophysiol* 91: 2164–2171, 2004.

Hasan Z. A model of spindle afferent response to muscle stretch. *J Neurophysiol* 49: 989–1006, 1983.

Hill DK. Tension due to interaction between the sliding filaments in resting striated muscle: the effect of stimulation. *J Physiol* 199: 637–684, 1968.

Houk JC, Rymer WZ, and Crago PE. Dependence of dynamic response of spindle receptors on muscle length and velocity. *J Neurophysiol* 46: 143–166, 1981.

Houk JC, Rymer WZ, and Crago PE. Responses of muscle spindle receptors to transitions in stretch velocity. In: *Muscle Afferents and Spinal Control of Movement*, edited by Jami L, Pierrot-Deseilligny E, and Zytnicki D. New York: Pergamon, 1992, p. 53–61.

Hulliger M. The mammalian muscles spindle and its central control. *Rev Physiol Biochem Pharmacol* 101: 1–110, 1984.

Hulliger M, Matthews PBC, and North J. Static and dynamic fusimotor action on the response of Ia fibers to low frequency sinusoidal stretching of widely ranging amplitude. *J Physiol* 267: 811–838, 1977a.

Hulliger M, Matthews PBC, and North J. Effects of combining static and dynamic fusimotor stimulation on the response of the muscle spindle primary ending to sinusoidal stretching. *J Physiol* 267: 839–856, 1977b.

Lan N, Song D, Mileusnic M, and Gordon J. Modeling spinal sensorimotor control for reach task. *IEEE Eng Med Biol Soc Abstr* 2484, 2005.

Lennerstrand G. Position and velocity sensitivity of muscle spindles in the cat. I. Primary and secondary endings deprived of fusimotor activation. *Acta Physiol Scand* 73: 281–299, 1968.

Lennerstand G and Thoden U. Position and velocity sensitivity of muscle spindles in the cat. II. Dynamic fusimotor single-fiber activation of primary endings. *Acta Physiol Scand* 74: 16–29, 1968a.

Lennerstand G and Thoden U. Position and velocity sensitivity of muscle spindles in the cat. III. Static fusimotor single-fiber activation of primary and secondary endings. *Acta Physiol Scand* 74: 30–49, 1968b.

Lin CK and Crago PE. Structural model of the muscle spindle. *Ann Biomed Eng* 30: 68–83, 2002.

Loeb GE. The control and responses of mammalian muscle spindles during normally executed motor tasks. *Exerc Sport Sci Rev* 12: 157–204, 1984.

Loeb GE and Duysens J. Activity patterns in individual hindlimb primary and secondary muscle spindle afferents during normal movements in unrestrained cats. *J Neurophysiol* 42: 420–440, 1979.

Loeb GE and Hoffer JA. Activity of spindle afferents from cat anterior thigh muscles. II. Effects of fusimotor blockade. *J Neurophysiol* 54: 565–577, 1985.

Loeb GE, Hoffer JA, and Pratt CA. Activity of spindle afferents form cat anterior thigh muscles. I. Identification and patterns during normal locomotion. *J Neurophysiol* 54: 549–564, 1985.

Loeb GE and Marks WB. Optimal control principles for sensory transducers. In: *Proceedings of the International Symposium: The Muscle Spindle*, edited by Boyd IA and Gladden MH. London: Macmillan, 1985, p. 409–415.

Lund JP, Smith AM, Sessle B, and Murakami T. Activity of trigeminal alpha and gamma motoneurons and muscle afferents during performance of a biting task. *J Neurophysiol* 42: 710–725, 1979.

Maltenfort MG and Burke RE. Spindle model responsive to mixed fusimotor inputs and testable predictions of beta feedback effects. *J Neurophysiol* 89: 2797–2809, 2003.

Matthews PBC. The differentiation of two types of fusimotor fiber by their effects on the dynamic response of muscle spindle primary endings. *Q J Exp Physiol* 47: 324–333, 1962.

Matthews PBC. The response of de-efferented muscle spindle receptors to stretching at different velocities. *J Physiol* 168: 660–678, 1963.

Matthews PBC. *Mammalian Muscle Receptors and Their Central Actions.* Baltimore, MD: Williams & Wilkins, 1972.

Matthews PBC. Evolving views on the internal operation and functional role of the muscle spindle. *J Physiol* 320: 1–30, 1981.

Matthews PBC and Stein RB. The sensitivity of muscle spindle afferents to small sinusoidal changes of length. *J Physiol* 200: 723–743, 1969.

McMahon TA. A lumped, linear model of the spindle. In: *Muscles, Reflexes, and Locomotion.* Princeton, NJ: Princeton Univ. Press, 1984, p. 152–154.

Mileusnic M, Lan N, and Loeb GE. Development of a muscle spindle model. *Soc Neurosci Abstr* 301.5, 2001.

Mileusnic M, Loeb GE, and Brown IE. Development of a muscle spindle model. *Int Funct Elec Stimul Soc Abstr* 106-MN05, 2002.

Murphy PR, Stein RB, and Taylor J. Phasic and tonic modulation of impulse rates in γ-motoneurons during locomotion in premammilary cats. *J Neurophysiol* 52: 228–243, 1984.

Nichols TR and Cope TC. Cross-bridge mechanics underlying the history-dependent properties of muscle spindles and stretch reflexes. *Can J Physiol Pharmacol* 82: 569–576, 2004.

Ovalle WK and Smith RS. Histochemical identification of three types of intrafusal muscle fibers in the cat and monkey based on the myosin ATPase reaction. *Can J Physiol Pharmacol* 50: 195–202, 1972.

Poppele RE and Quick DC. Stretch-induced contraction of intrafusal muscle in cat muscle spindle. *J Neurosci* 1: 1069–1074, 1981.

Press WH, Flannery BP, Teukolsky SA, and Vetterling WT. *Numerical Recipes.* Cambridge, UK: Cambridge Univ. Press, 1986.

Prochazka A. Proprioceptive feedback and movement regulation. In: *Handbook of Physiology. Exercise: Regulation and Integration of Multiple Systems. Neural Control of Movement*. Bethesda, MD: Am. Physiol. Soc., 1996, sect. 12, p. 89–127.

Prochazka A and Gorassini M. Models of ensemble firing of muscle spindle afferents recorded during normal locomotion in cats. *J Physiol* 507: 277–291, 1998.

Proske U and Gregory E. Signaling properties of muscle spindles and tendon organs. In: *Sensorimotor Control of Movement and Posture*, edited by Gandevia SC, Proske U, and Stuart DG. New York: Kluwer Academic/Plenum, 2002, p. 1–8.

Proske U and Morgan DL. Do cross-bridges contribute to the tension during stretch of passive muscle? *J Muscle Res Cell Motil* 20: 433–442, 1999.

Rudjord T. A second order mechanical model of muscle spindle primary endings. *Kybernetik* 6: 205–213, 1970.

Schaafsma A, Otten E, and Van Willigen JD. A muscle spindle model for primary afferent firing based on a simulation of intrafusal mechanical events. *J Neurophysiol* 65: 1297–1312, 1991.

Scheepstra KA, Otten E, Hulliger M, and Banks RW. Modeling of chaotic and regular Ia afferent discharge during fusimotor stimulation. In: *Alpha and Gamma Motor Systems*, edited by Taylor A, Gladden MH, and Durbaba R. New York: Plenum Press, 1995, p. 325–327.

Scott SH, Brown IE, and Loeb GE. Mechanics of feline soleus. I. Effect of fascicle length and velocity on force output. *J Muscle Res Cell Motil* 17: 207–219, 1996.

Scott SH and Loeb GE. The computation of position sense from spindle in mono- and multiarticular muscles. *J Neurosci* 14: 7529–7540, 1994.

Taylor A, Elleway PH, Durbaba R, and Rawlinson S. Distinctive patterns of static and dynamic gamma motor activity during locomotion in the decerebrate cat. *J Physiol* 529: 825–836, 2000.

Downloaded from jn.physiology.org on September 18, 2006